

Cross-Spectral Analysis of Bivariate Graph Signals

KYUSOON KIM AND HEE-SEOK OH

Seoul National University, Seoul 08826, Korea

August 13, 2024

Abstract

With the advancements in technology and monitoring tools, we often encounter multivariate graph signals, which can be seen as the realizations of multivariate graph processes, and revealing the relationship between their constituent quantities is one of the important problems. To address this issue, we propose a cross-spectral analysis tool for bivariate graph signals. The main goal of this study is to extend the scope of spectral analysis of graph signals to multivariate graph signals. In this study, we define joint weak stationarity graph processes and introduce graph cross-spectral density and coherence for multivariate graph processes. We propose several estimators for the cross-spectral density and investigate the theoretical properties of the proposed estimators. Furthermore, we demonstrate the effectiveness of the proposed estimators through numerical experiments, including simulation studies and a real data application. Finally, as an interesting extension, we discuss robust spectral analysis of graph signals in the presence of outliers.

Keywords: Bivariate graph signal; Cross-spectral density; Cross-spectrum; Periodogram; Random graph process.

1 Introduction

Graph signals, defined on nodes (or vertices) in a graph (or network), have become popular in various fields, such as signal processing, environmental science, economics, and sociology.

Many studies have focused on developing deterministic graph signal processing tools, covering topics such as sampling and recovery (Chen et al., 2015a,b; Lorenzo et al., 2018; Narang and Ortega, 2011; Tanaka, 2018), graph filter and filter bank design (Anis and Ortega, 2017; Narang and Ortega, 2012; Sakiyama and Tanaka, 2014; Tremblay et al., 2018), representation (Bulai and Salianni, 2023; Crovella and Kolaczyk, 2003; Hammond et al., 2011; Narang and Ortega, 2009; Sandryhaila and Moura, 2013b), and denoising (Onuki et al., 2016; Stankovic et al., 2019; Waheed and Tay, 2018). More recently, statistical graph signal processing, which uses a probabilistic approach to deal with random graph processes, has gained attention. In statistical graph signal processing, as in classical signal processing, the notion of stationarity is fundamental and has been defined on graphs in several works of literature (Girault, 2015b; Perraudin and Vandergheynst, 2017; Segarra et al., 2016). Stationary graph processes can be characterized by their graph power spectral density in the graph frequency domain, which can facilitate understanding, model building, and prediction of these processes.

Spectral analysis using graph power spectral density is typically limited to univariate graph processes. However, we often encounter multivariate graph processes in the real world, such as RGB signals on pixels, meteorological data from environmental sensor networks, economic indicators in trading networks, and brain network responses to stimuli. For these multivariate graph signals, we are interested in investigating interrelationships between the processes, such as their correlation and shared information, which are not readily apparent from analyzing individual spectra. In classical signal processing, this type of analysis is called cross-spectral analysis (Fuller, 2009; Priestley, 1982; Von Storch and Zwiers, 2002). The main contribution of this study is the development of a cross-spectral analysis framework on graphs. Specifically, we extend the works of Segarra et al. (2016) and Perraudin and Vandergheynst (2017) to analyze multivariate graph processes. We define the notions of joint weak stationarity and cross-spectral density on graphs. We then propose several nonparametric estimators for the graph cross-spectral density and provide theoretical properties. Finally, we demonstrate the effectiveness of the proposed estimators through numerical experiments.

The remainder of this paper is organized as follows. In Section 2, we review the graph

spectral theory and the concepts of weakly stationary graph processes and power spectral density on graphs. Several nonparametric estimators for the graph power spectral density are also introduced in this section. In Section 3, we define the notions of joint weak stationarity, cross-spectral density, and coherence on graphs. In addition, we propose estimators for the cross-spectral density and investigate their theoretical properties. Section 5 conducts numerical experiments on various graphs. In Section 6, we discuss a robust spectral analysis on graphs, proposing M -type estimators for the graph power spectral density and graph cross-spectral density. Concluding remarks are provided in Section 7. The proofs of theoretical properties in Section 3 are given in Appendix A. R codes to reproduce the numerical experiments can be available at <https://github.com/qsoon/graph-cross-spectral-analysis>.

2 Preliminary

2.1 Graph spectral theory and notations

Let $\mathcal{G} = (\mathcal{V}, \mathcal{E}, \mathbf{A})$ be an undirected or a directed weighted graph with a set of N nodes \mathcal{V} (i.e., $|\mathcal{V}| = N$), a set of edges \mathcal{E} , and a weighted adjacency matrix $\mathbf{A} = (A_{i,j})_{N \times N}$ whose entry $A_{i,j} \neq 0$ only if the i th node and the j th node are connected. Denote a graph shift operator (GSO) by a matrix $\mathbf{S} = (S_{i,j})_{N \times N}$, which is a local operator that replaces a signal value x_i at the i th node of a graph signal $\mathbf{x} = (x_1, \dots, x_N)^\top \in \mathbb{R}^N$ with a linear combination of signal values at neighboring nodes of the i th node (Sandryhaila and Moura, 2013a, 2014; Segarra et al., 2018). The entry of GSO, $S_{i,j}$, is nonzero only if $i = j$ or the i th node and the j th node are connected, so GSO contains information on the local structure of graph \mathcal{G} . The adjacency matrix \mathbf{A} and the graph Laplacian $\mathbf{L} := \mathbf{D} - \mathbf{A}$ (where \mathbf{D} is a diagonal matrix with $D_{i,i} = \sum_{j=1}^N A_{i,j}$) are examples of GSO. If \mathbf{S} is normal (i.e., $\mathbf{S}^H \mathbf{S} = \mathbf{S} \mathbf{S}^H$, where \mathbf{S}^H denotes the conjugate transpose of \mathbf{S}), the spectral theorem states that there exists a unitary matrix \mathbf{V} (i.e., $\mathbf{V}^H \mathbf{V} = \mathbf{V} \mathbf{V}^H = \mathbf{I}$) such that $\mathbf{S} = \mathbf{V} \mathbf{\Lambda} \mathbf{V}^H$ with a diagonal matrix $\mathbf{\Lambda}$. The entries of $\mathbf{\Lambda}$ need not be real, whereas they are real if \mathbf{S} is Hermitian (i.e., $\mathbf{S}^H = \mathbf{S}$). In this study, we only consider real-valued graph signals and normal GSOs.

Given a normal GSO \mathbf{S} and a graph signal $\mathbf{x} \in \mathbb{R}^N$, the graph Fourier transform (GFT) is defined as $\tilde{\mathbf{x}} = \mathbf{V}^H \mathbf{x}$, which is referred to as the graph Fourier coefficients or spectrum coefficients of \mathbf{x} (Sandryhaila and Moura, 2013b). GFT represents a graph signal in terms of frequencies by transforming the signal from the node domain to the graph spectral domain. Throughout this paper, $\langle \cdot \rangle$, \circ , $\langle\langle \cdot, \cdot \rangle\rangle$, and $*$ denote the inner product, the elementwise product, the elementwise inner product, and the elementwise conjugate, respectively. That is, $\langle\langle \boldsymbol{\xi}, \boldsymbol{\zeta} \rangle\rangle = \boldsymbol{\xi} \circ \boldsymbol{\zeta}^*$ for $\boldsymbol{\xi}$ and $\boldsymbol{\zeta}$, which are complex-valued vectors. Furthermore, $|\cdot|^2$ is applied elementwise.

2.2 Weakly stationary graph processes

In statistical graph signal processing, we consider a graph signal \mathbf{x} to be a realization of a random graph process X . Since weak stationarity plays a vital role in statistical signal processing, it is a priority to establish the notion of weak stationarity for graph processes. Defining weak stationarity on graphs is challenging due to the absence of directional concepts, making it difficult to define notions such as translation and lag. Several studies have been done to define the weak stationarity of graph processes. Girault (2015b) and Girault (2015a) pioneered a definition of weak stationarity for graph processes based on an isometric graph translation operator, which preserves the signal’s energy and is isometric, unlike the GSOs. They defined a weakly stationary graph process as one whose first and second moments remain invariant under multiplications with the isometric translation. However, this new translation operator does not have localization properties essential to the stationarity concept.

Perraudin and Vandergheynst (2017) proposed an alternative definition of weakly stationary graph processes using graph Laplacian as a localization operator on graphs. Marques et al. (2017) and Segarra et al. (2018) extended this definition, generalizing it to normal GSOs, thus not restricting it to the graph Laplacian. They suggested three equivalent definitions (under mild conditions) as follows.

Definition 2.1. (Marques et al., 2017) Given a normal shift operator \mathbf{S} , a zero-mean random graph process X is weakly stationary with respect to \mathbf{S} if one of the following

holds:

- (a) The graph process X can be expressed as the response of the linear shift-invariant graph filter $\mathbf{H} = \sum_{\ell=0}^{N-1} h_{\ell} \mathbf{S}^{\ell}$ to a zero-mean white input $\boldsymbol{\epsilon}$ (i.e., $E(\boldsymbol{\epsilon}) = \mathbf{0}$ and $E(\boldsymbol{\epsilon}\boldsymbol{\epsilon}^H) = \mathbf{I}$).
- (b) For any set of non-negative integers a , b , and $c \leq b$, it holds that

$$E\left((\mathbf{S}^a X)((\mathbf{S}^H)^b X)^H\right) = E\left((\mathbf{S}^{a+c} X)((\mathbf{S}^H)^{b-c} X)^H\right)$$

- (c) The covariance matrix $\boldsymbol{\Sigma}_X = E(XX^H)$ and \mathbf{S} are simultaneously diagonalizable.

Remark 2.1. It is known that a graph filter is linear shift-invariant if and only if it is a polynomial in the graph shift (Sandryhaila and Moura, 2013a). It is also worth noting that Definition 2.1(a) gives a constructive definition of weak stationarity. Definition 2.1(b) and (c) generalize the definition of weak stationarity in classical signal processing. The former corresponds to the requirement that the second moment of a weakly stationary process is invariant to time shifts, and the latter corresponds to the requirement that the covariance of a weakly stationary process must be circulant.

Remark 2.2. If X is not a zero-mean process, it is required to have the first moment of the form $E(X) = \alpha \mathbf{v}_k$ for a constant α and $1 \leq k \leq N$ to satisfy weak stationarity with respect to $\mathbf{S} = \mathbf{V}\boldsymbol{\Lambda}\mathbf{V}^H$ for $\mathbf{V} = (\mathbf{v}_1 | \dots | \mathbf{v}_N)$ (Marques et al., 2017; Segarra et al., 2016). If $\mathbf{S} = \mathbf{L}$ and $k = 1$, $E(X)$ becomes a constant signal. In other literature, Girault (2015b) required $E(X)$ to be a zero vector, while Perraudin and Vandergheynst (2017) required it to be $\alpha \mathbf{1}$.

Proposition 2.1. (Marques et al., 2017) *Definition 2.1(b) and (c) are equivalent. Furthermore, if the eigenvalues of \mathbf{S} are all distinct, all three definitions in Definition 2.1 are equivalent.*

Proof. The proofs can be found in Marques et al. (2017). □

2.3 Graph power spectral density

To describe the energy distribution of a weakly stationary graph process over frequency, we can define the *graph power spectral density* (GPSD) in Definition 2.2 (Marques et al., 2017; Perraudin and Vandergheynst, 2017; Segarra et al., 2016). We assume that GSO \mathbf{S} is normal, and the appearing graph processes are real-valued and zero-mean. For consistency, we will continue to use the notation H or $*$ when dealing with real-valued vectors.

Definition 2.2. (Marques et al., 2017) The graph power spectral density of a zero-mean weakly stationary graph process X is defined as a non-negative $N \times 1$ vector $\mathbf{p}_X = \text{diag}(\mathbf{V}^H \boldsymbol{\Sigma}_X \mathbf{V})$.

Remark 2.3. If X is weakly stationary with respect to $\mathbf{S} = \mathbf{V} \boldsymbol{\Lambda} \mathbf{V}^H$, the covariance matrix $\boldsymbol{\Sigma}_X$ and \mathbf{S} are simultaneously diagonalizable by Definition 2.1(c). Therefore, we can rewrite $\boldsymbol{\Sigma}_X = \mathbf{V} \text{diag}(\mathbf{p}_X) \mathbf{V}^H$. Moreover, since $\boldsymbol{\Sigma}_X$ is Hermitian, \mathbf{p}_X is a real-valued vector.

We note that $\mathbf{p}_X = \text{diag}(\mathbf{V}^H \boldsymbol{\Sigma}_X \mathbf{V}) = E(|\mathbf{V}^H X|^2) = E(|\tilde{X}|^2)$, which implies GPSD indicates the energy distribution over graph frequencies. Thus, we can interpret the ℓ th element of \mathbf{p}_X as $(\mathbf{p}_X)_\ell =: \mathbf{p}_X(\lambda_\ell)$, where λ_ℓ ($1 \leq \ell \leq N$) are the eigenvalues of \mathbf{S} .

2.4 Nonparametric estimation of graph power spectral density

2.4.1 Graph periodogram

Assuming that we have R realizations $\{\mathbf{x}_r\}_{r=1}^R$ of a weakly stationary graph process X in $\mathbf{S} = \mathbf{V} \boldsymbol{\Lambda} \mathbf{V}^H$, Marques et al. (2017) proposed three nonparametric estimators of GPSD that follow naturally from Definition 2.2: periodogram, correlogram, and least squares types. The periodogram-type estimator is defined as

$$\hat{\mathbf{p}}_X^p = \frac{1}{R} \sum_{r=1}^R |\tilde{\mathbf{x}}_r|^2 = \frac{1}{R} \sum_{r=1}^R |\mathbf{V}^H \mathbf{x}_r|^2,$$

where $\tilde{\mathbf{x}}_r$ denotes the graph Fourier coefficients of \mathbf{x}_r . The correlogram-type estimator is defined as

$$\hat{\mathbf{p}}_X^c = \text{diag}(\mathbf{V}^H \hat{\Sigma}_X \mathbf{V}),$$

where $\hat{\Sigma}_X = \frac{1}{R} \sum_{r=1}^R \mathbf{x}_r \mathbf{x}_r^H$. These two estimators are analogous to the periodogram and correlogram of time signals in classical signal processing. Finally, for $\mathbf{G} = (\text{vec}(\mathbf{v}_1 \mathbf{v}_1^H) | \cdots | \text{vec}(\mathbf{v}_N \mathbf{v}_N^H))$, the least squares estimator is defined as

$$\hat{\mathbf{p}}_X^{ls} = \arg \min_p \|\hat{\sigma}_X - \mathbf{G} \mathbf{p}\|_2^2 = (\mathbf{G}^H \mathbf{G})^{-1} \mathbf{G}^H \hat{\sigma}_X, \quad (1)$$

where $\hat{\sigma}_X = \text{vec}(\hat{\Sigma}_X)$.

Proposition 2.2. (Segarra et al., 2018) *For a zero-mean weakly stationary graph process X , the three GPSD estimators are identical, i.e.,*

$$\hat{\mathbf{p}}_X^p = \hat{\mathbf{p}}_X^c = \hat{\mathbf{p}}_X^{ls}.$$

Hence, we refer to the three estimators as *graph periodogram* and denote them by $\hat{\mathbf{p}}_X$.

2.4.2 Windowed average graph periodogram

It is known that the bias of the graph periodogram $\hat{\mathbf{p}}_X$ is zero, but its covariance is equal to $(2/R) \text{diag}^2(\mathbf{p}_X)$ when the process X is Gaussian and \mathbf{S} is symmetric, resulting in MSE of the graph periodogram being $(2/R) \|\mathbf{p}_X\|_2^2$ (Marques et al., 2017). Therefore, the number of realizations R significantly affects the estimation performance. As R increases, the graph periodogram tends to get closer to the true GPSD, while small R degrades the estimation performance. However, obtaining multiple realizations of the graph process is often impractical. In classical signal processing, the issue of having only one or a few realizations can be effectively tackled using data windows, such as Bartlett's method (Bartlett, 1950) and Welch's method (Welch, 1967), or lag windows, such as Blackman–Tukey method (Blackman and Tukey, 1959). Similarly, for graph signals, windows can be utilized to estimate GPSD when only one or a few realizations are available.

Marques et al. (2017) proposed a windowed average graph periodogram when one realization \mathbf{x} is available. They introduced a data window $\mathbf{w} \in \mathbb{R}^N$ satisfying $\|\mathbf{w}\|_2^2 = \|\mathbf{1}\|_2^2 = N$, and then defined a windowed graph periodogram, for a windowed signal $\mathbf{x}_w = \text{diag}(\mathbf{w})\mathbf{x}$, as

$$\hat{\mathbf{p}}_X^w = |\mathbf{V}^H \mathbf{x}_w|^2 = |\tilde{\mathbf{W}} \mathbf{V}^H \mathbf{x}|^2,$$

where $\tilde{\mathbf{W}} = \mathbf{V}^H \mathbf{W} \mathbf{V}$. To generate multiple signals from one realization, they utilized a bank of M windows, $\mathcal{W} = \{\mathbf{w}_m\}_{m=1}^M$. A windowed average graph periodogram is then defined as

$$\hat{\mathbf{p}}_X^{\mathcal{W}} = \frac{1}{M} \sum_{m=1}^M \hat{\mathbf{p}}_X^{w_m}. \quad (2)$$

3 Cross-spectral analysis on graphs

3.1 Jointly weakly stationary graph processes

First, we define the notion of joint weak stationarity on graphs for cross-spectral analysis. This notion can be straightforwardly extended from Definition 2.1 as follows.

Definition 3.1. Given a normal shift operator $\mathbf{S} = \mathbf{V} \mathbf{\Lambda} \mathbf{V}^H$, if zero-mean random graph processes X and Y are both weakly stationary with respect to \mathbf{S} and one of the following holds, then X and Y are jointly weakly stationary with respect to \mathbf{S} :

- (a) Graph processes X and Y can be expressed as the responses of two linear shift-invariant graph filters $\mathbf{H}_1 = \sum_{\ell=0}^{N-1} h_{1,\ell} \mathbf{S}^\ell$ and $\mathbf{H}_2 = \sum_{\ell=0}^{N-1} h_{2,\ell} \mathbf{S}^\ell$ to zero-mean white inputs $\boldsymbol{\epsilon}_1$ and $\boldsymbol{\epsilon}_2$, where the cross-covariance $\mathbf{V}^H \text{Cov}(\boldsymbol{\epsilon}_1, \boldsymbol{\epsilon}_2) \mathbf{V}$ is diagonal.
- (b) For any set of non-negative integers a , b , and $c \leq b$, it holds that

$$E\left((\mathbf{S}^a X)((\mathbf{S}^H)^b Y)^H\right) = E\left((\mathbf{S}^{a+c} X)((\mathbf{S}^H)^{b-c} Y)^H\right)$$

- (c) The cross-covariance matrix $\boldsymbol{\Sigma}_{XY} = E(XY^H)$ and \mathbf{S} are simultaneously diagonalizable.

Remark 3.1. We note that Definition 3.1 differs from the notion of jointly wide-sense stationarity proposed by Loukas and Perraudin (2019), which dealt with time-varying processes defined over graphs. Their terms “jointly wide-sense stationarity” and “time-vertex wide-sense stationarity” imply that a process is multivariate time-wide-sense stationary and multivariate vertex-wide-sense stationary, respectively. Here, the definition of multivariate vertex-wide-sense stationarity is the same as Definition 3.1(c); however, Definition 3.1 provides additional equivalent definitions, including Definition 3.1(a), which offers a constructive definition of joint weak stationarity. Moreover, in their work, the concept of joint power spectral density as a function of graph frequency and angular frequency represents the energy distribution in the joint frequency domain. This differs from the graph cross-spectral density described in Section 3.2, which represents the energy distribution between two signals as a function of graph frequency.

Remark 3.2. Since $\Sigma_{XY} = (\Sigma_{YX})^H$, Definition 3.1(c) is equivalent to that Σ_{YX} and \mathbf{S} are simultaneously diagonalizable.

Remark 3.3. Similar to Remark 2.2, if X and Y are not zero-mean processes, they are required to have the first moments of the forms $E(X) = \alpha \mathbf{v}_k$ and $E(Y) = \beta \mathbf{v}_\ell$ for some constants α and β and $1 \leq k, \ell \leq N$ to satisfy joint weak stationarity with respect to $\mathbf{S} = \mathbf{V} \Lambda \mathbf{V}^H$. Recall that the graph processes considered in this study are assumed to be real-valued and zero-mean.

Remark 3.4. Perraudin and Vandergheynst (2017) and Marques et al. (2017) discussed a measure of weak stationarity as $\|\text{diag}(\mathbf{V}^H \hat{\Sigma}_X \mathbf{V})\|_2 / \|\mathbf{V}^H \hat{\Sigma}_X \mathbf{V}\|_F$ for the estimated covariance matrix $\hat{\Sigma}_X$. In a similar vein, the joint weak stationarity level can be measured using the computed measure $\|\text{diag}(\mathbf{V}^H \hat{\Sigma}_{XY} \mathbf{V})\|_2 / \|\mathbf{V}^H \hat{\Sigma}_{XY} \mathbf{V}\|_F$ for the estimated cross-covariance matrix $\hat{\Sigma}_{XY}$, where $\|\cdot\|_F$ denotes the Frobenius norm. The closer this measure is to 1, the more the two graph processes are jointly weakly stationary.

Proposition 3.1. *Definition 3.1(b) and (c) are equivalent. Furthermore, if the eigenvalues of \mathbf{S} are all distinct, all three definitions in Definition 3.1 are equivalent.*

A proof of Proposition 3.1 is provided in Appendix A.

3.2 Graph cross-spectral density

Like power spectral density, cross-spectral density (CSD) is a function of frequency. It describes the frequencies shared between two signals and provides information about the correlation of the two signals in the frequency domain. Extending the notion of CSD in classical signal processing, we define a graph cross-spectral density (GCSD) based on the definition of the graph power spectral density.

Definition 3.2. The graph cross-spectral density of zero-mean weakly stationary graph processes X and Y is defined as an $N \times 1$ vector $\mathbf{p}_{XY} = \text{diag}(\mathbf{V}^H \boldsymbol{\Sigma}_{XY} \mathbf{V})$.

Remark 3.5. If X and Y are jointly weakly stationary with respect to $\mathbf{S} = \mathbf{V} \boldsymbol{\Lambda} \mathbf{V}^H$, the cross-covariance matrix $\boldsymbol{\Sigma}_{XY}$ and \mathbf{S} are simultaneously diagonalizable by Definition 3.1(c). Thus, we can rewrite $\boldsymbol{\Sigma}_{XY} = \mathbf{V} \text{diag}(\mathbf{p}_{XY}) \mathbf{V}^H$. Unlike GPSD, $\boldsymbol{\Sigma}_{XY}$ can be a complex-valued vector because $\boldsymbol{\Sigma}_{XY}$ is not required to be Hermitian.

In addition, according to Remark 3.2, an alternative definition of GCSD can be formulated as $\mathbf{p}_{YX} = \text{diag}(\mathbf{V}^H \boldsymbol{\Sigma}_{YX} \mathbf{V})$. Since $\boldsymbol{\Sigma}_{XY} = (\boldsymbol{\Sigma}_{YX})^H$, the relationship between the two definitions is $\mathbf{p}_{XY} = \mathbf{p}_{YX}^*$. As a result, we adopt \mathbf{p}_{XY} as the definition of GCSD because they contain the same information.

We present three propositions analogous to Property 1, Property 2, and Property 3 in Segarra et al. (2016).

Proposition 3.2. *Let X and Y be zero-mean jointly weakly stationary processes with cross-covariance $\boldsymbol{\Sigma}_{XY}$ and GCSD \mathbf{p}_{XY} . Consider two filters \mathbf{H}_1 and \mathbf{H}_2 with frequency responses $\tilde{\mathbf{h}}_1 = \text{diag}(\mathbf{V}^H \mathbf{H}_1 \mathbf{V})$ and $\tilde{\mathbf{h}}_2 = \text{diag}(\mathbf{V}^H \mathbf{H}_2 \mathbf{V})$, respectively, and define $Z = \mathbf{H}_1 X$ and $W = \mathbf{H}_2 Y$. Then,*

(a) Z and W are jointly stationary in \mathbf{S} with cross-covariance $\boldsymbol{\Sigma}_{ZW} = \mathbf{H}_1 \boldsymbol{\Sigma}_{XY} \mathbf{H}_2^H$.

(b) Z and W have GCSD $\mathbf{p}_{ZW} = \tilde{\mathbf{h}}_1 \circ \tilde{\mathbf{h}}_2^* \circ \mathbf{p}_{XY}$.

Proposition 3.3. *Let X and Y be zero-mean random graph processes that are outputs of linear shift-invariant graph filters \mathbf{H}_1 and \mathbf{H}_2 of degree $L_1 - 1$ and $L_2 - 1$, respectively, applied to white inputs $\boldsymbol{\epsilon}_1$ and $\boldsymbol{\epsilon}_2$, where $\text{Cov}(\boldsymbol{\epsilon}_1, \boldsymbol{\epsilon}_2) = \mathbf{I}$. Then, if the distance between the i th node and the j th node is greater than $(L_1 + L_2 - 2)$ hops, $(\boldsymbol{\Sigma}_{XY})_{i,j} = 0$.*

Proposition 3.4. *Given zero-mean jointly weakly stationary graph processes X and Y with GCSD \mathbf{p}_{XY} , define GFT processes as $\tilde{X} = \mathbf{V}^H X$ and $\tilde{Y} = \mathbf{V}^H Y$. Then, \tilde{X} and \tilde{Y} are uncorrelated, and its cross-covariance is*

$$\boldsymbol{\Sigma}_{\tilde{X}\tilde{Y}} = E(\tilde{X}\tilde{Y}^H) = \text{diag}(\mathbf{p}_{XY}).$$

Proposition 3.2 is the counterpart of the spectral convolution theorem for graph processes. Proposition 3.3 represents a limitation of cross-correlations between signal values generated by specific filtering, which is beneficial in designing windows for the windowed average graph cross-periodogram in Section 3.3.2 when combined with the results of Proposition 3.9. In addition, Proposition 3.4 highlights the usefulness of graph frequency domain analysis. Proofs for the above propositions are found in Appendix A.

3.3 Nonparametric estimation of graph cross-spectral density

3.3.1 Graph cross-periodogram

We propose three nonparametric estimators of GCSD, assuming that we have R realizations $\mathbf{x}_1, \dots, \mathbf{x}_R$ and $\mathbf{y}_1, \dots, \mathbf{y}_R$ of processes X and Y , respectively. To emphasize the correspondence between the proposed estimates and those introduced in Section 2.4.1, we present periodogram, correlogram, and least squares types. A periodogram-type estimator is defined as

$$\hat{\mathbf{p}}_{XY}^p = \frac{1}{R} \sum_{r=1}^R \langle\langle \tilde{\mathbf{x}}_r, \tilde{\mathbf{y}}_r \rangle\rangle = \frac{1}{R} \sum_{r=1}^R (\mathbf{V}^H \mathbf{x}_r) \circ (\mathbf{V}^H \mathbf{y}_r)^*,$$

where $\tilde{\mathbf{x}}_r$ and $\tilde{\mathbf{y}}_r$ are graph Fourier coefficients of \mathbf{x}_r and \mathbf{y}_r , respectively. A correlogram-type estimator is defined as

$$\hat{\mathbf{p}}_{XY}^c = \text{diag}(\mathbf{V}^H \hat{\boldsymbol{\Sigma}}_{XY} \mathbf{V}),$$

where the sample cross-covariance $\hat{\Sigma}_{XY} = \frac{1}{R} \sum_{r=1}^R \mathbf{x}_r \mathbf{y}_r^H$. Finally, considering $\Sigma_{XY} = \mathbf{V} \text{diag}(\mathbf{p}_{XY}) \mathbf{V}^H = \sum_{i=1}^N (\mathbf{p}_{XY})_i \mathbf{v}_i \mathbf{v}_i^H$, we define a least squares estimator as

$$\hat{\mathbf{p}}_{XY}^{ls} = \arg \min_{\mathbf{p}} \|\hat{\sigma}_{XY} - \mathbf{G}\mathbf{p}\|_2^2 = (\mathbf{G}^H \mathbf{G})^{-1} \mathbf{G}^H \hat{\sigma}_{XY}, \quad (3)$$

where $\mathbf{G} = (\text{vec}(\mathbf{v}_1 \mathbf{v}_1^H) | \dots | \text{vec}(\mathbf{v}_N \mathbf{v}_N^H))$ and $\hat{\sigma}_{XY} = \text{vec}(\hat{\Sigma}_{XY})$.

Proposition 3.5. *For zero-mean jointly weakly stationary graph processes X and Y , the three different GCSD estimators are identical, i.e.,*

$$\hat{\mathbf{p}}_{XY}^p = \hat{\mathbf{p}}_{XY}^c = \hat{\mathbf{p}}_{XY}^{ls}.$$

A proof of Proposition 3.5 is provided in Appendix A. Hence, we refer to the three estimators as *graph cross-periodogram* and denote them by $\hat{\mathbf{p}}_{XY}$.

Proposition 3.6. *For zero-mean jointly weakly stationary graph processes X and Y with GCSD \mathbf{p}_{XY} , the bias and the variance of the graph cross-periodogram $\hat{\mathbf{p}}_{XY}$ are computed as follows:*

(a) $E(\hat{\mathbf{p}}_{XY}) = \mathbf{p}_{XY}$.

(b) *If X and Y are Gaussian and \mathbf{S} is symmetric, $\text{Var}(\hat{\mathbf{p}}_{XY}) = \frac{1}{R} (\text{diag}(|\mathbf{p}_{XY}|^2) + \text{diag}(\mathbf{p}_X) \text{diag}(\mathbf{p}_Y))$, where \mathbf{p}_X and \mathbf{p}_Y are the GPSDs of X and Y , respectively.*

Remark 3.6. If $X = Y$, then the results in Proposition 3.6 reduce to those of the periodogram described in Marques et al. (2017).

Proposition 3.6 implies that the MSE of the graph cross-periodogram decreases as the number of realizations R increases. The bottom panel of Figure 1 shows the effect of R on the performance of the graph cross-periodogram evaluated using the Karate club network (Zachary, 1977) in the top panel of Figure 1. To generate jointly weakly stationary graph processes, we utilize Definition 3.1(a). Specifically, we generate a white input ϵ from $N(0, 1)$ and then apply two linear shift-invariant filters, \mathbf{H}_{Mex} and \mathbf{H}_{heat} , with frequency responses defined as $\tilde{h}_{\text{Mex}}(\lambda) = 5\lambda e^{-25\lambda^2}$ and $\tilde{h}_{\text{heat}}(\lambda) = e^{-10\lambda}$, respectively. Here, λ

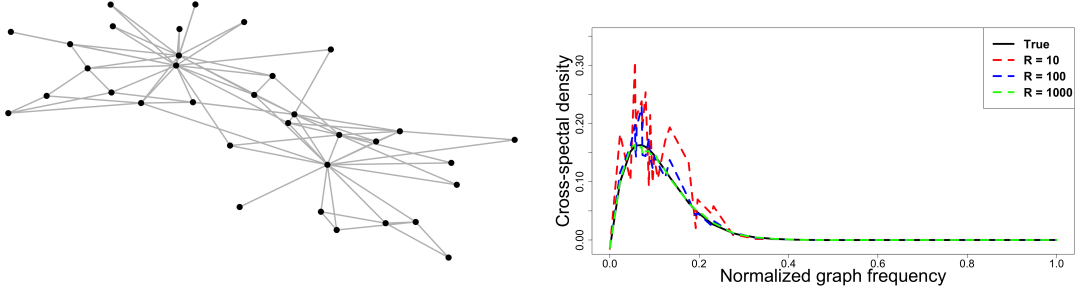


Figure 1: The Karate club network (left) and graph cross-periodograms for different values of R on the Karate club network (right).

denotes the normalized graph frequency in the interval $[0, 1]$. For implementation, we use the Chebyshev polynomial approximation Phillips (2006) to approximate these filters with a polynomial form $\mathbf{H} = \sum_{\ell=1}^{N-1} h_{\ell} \mathbf{S}^{\ell}$, where the graph Laplacian serves as a graph shift operator \mathbf{S} in the analysis. The true GCSD can be evaluated as $\tilde{h}_{\text{Mex}}(\lambda) \tilde{h}_{\text{heat}}^*(\lambda)$ by Proposition 3.2. As expected from Proposition 3.6, the accuracy of the graph cross-periodogram in estimating the true GCSD improves as R increases.

3.3.2 Windowed average graph cross-periodogram

As discussed in Section 2.4.2, utilizing multiple realizations of graph processes to estimate GCSD is impractical, so a data window can be adopted. Given realizations \mathbf{x} and \mathbf{y} of the processes X and Y , with a data window $\mathbf{w} \in \mathbb{R}^N$ such that $\|\mathbf{w}\|_2^2 = N$, we define a windowed graph cross-periodogram as

$$\hat{\mathbf{p}}_{\mathbf{x}\mathbf{y}}^{\mathbf{w}} = \langle\langle \mathbf{V}^H \mathbf{x}_{\mathbf{w}}, \mathbf{V}^H \mathbf{y}_{\mathbf{w}} \rangle\rangle = \langle\langle \mathbf{V}^H \text{diag}(\mathbf{w}) \mathbf{x}, \mathbf{V}^H \text{diag}(\mathbf{w}) \mathbf{y} \rangle\rangle = \langle\langle \tilde{\mathbf{W}} \mathbf{V}^H \mathbf{x}, \tilde{\mathbf{W}} \mathbf{V}^H \mathbf{y} \rangle\rangle,$$

where $\mathbf{x}_{\mathbf{w}} = \text{diag}(\mathbf{w}) \mathbf{x}$ and $\mathbf{y}_{\mathbf{w}} = \text{diag}(\mathbf{w}) \mathbf{y}$ denote windowed signals, and $\tilde{\mathbf{W}} = \mathbf{V}^H \text{diag}(\mathbf{w}) \mathbf{V}$ is defined as the dual of the windowing operator $\text{diag}(\mathbf{w})$ in the graph frequency domain.

The following proposition shows that the windowed graph cross-periodogram $\hat{\mathbf{p}}_{\mathbf{x}\mathbf{y}}^{\mathbf{w}}$ is biased unlike the graph cross-periodogram $\hat{\mathbf{p}}_{\mathbf{x}\mathbf{y}}$.

Proposition 3.7. *Let $\mathbf{p}_{\mathbf{x}\mathbf{y}}$ be the GCSD of zero-mean jointly weakly stationary graph*

processes X and Y . The expectation of the windowed graph cross-periodogram is

$$E(\hat{\mathbf{p}}_{XY}^{\mathbf{w}}) = (\tilde{\mathbf{W}} \circ \tilde{\mathbf{W}}^*) \mathbf{p}_{XY}.$$

A proof is given in Appendix A. By utilizing multiple windows from a window bank $\mathcal{W} = \{\mathbf{w}_m\}_{m=1}^M$, we define a windowed average graph cross-periodogram as

$$\hat{\mathbf{p}}_{XY}^{\mathcal{W}} = \frac{1}{M} \sum_{m=1}^M \hat{\mathbf{p}}_{XY}^{\mathbf{w}_m} = \frac{1}{M} \sum_{m=1}^M \langle\langle \tilde{\mathbf{W}}_m \mathbf{V}^H \mathbf{x}, \tilde{\mathbf{W}}_m \mathbf{V}^H \mathbf{y} \rangle\rangle,$$

where $\tilde{\mathbf{W}}_m = \mathbf{V}^H \text{diag}(\mathbf{w}_m) \mathbf{V}$.

Proposition 3.8. *Let X and Y be zero-mean jointly weakly stationary graph processes X and Y with GCSD \mathbf{p}_{XY} , and $\mathcal{W} = \{\mathbf{w}_m\}_{m=1}^M$. Then, the bias and the variance of the windowed average graph cross-periodogram $\hat{\mathbf{p}}_{XY}^{\mathcal{W}}$ are as follows:*

(a) $E(\hat{\mathbf{p}}_{XY}^{\mathcal{W}}) = \frac{1}{M} \sum_{m=1}^M (\tilde{\mathbf{W}}_m \circ \tilde{\mathbf{W}}_m^*) \mathbf{p}_{XY}.$

(b) *If X and Y are Gaussian and \mathbf{S} is symmetric,*

$$\text{tr}(\text{Var}(\hat{\mathbf{p}}_{XY}^{\mathcal{W}})) = \frac{1}{M^2} \sum_{m=1}^M \sum_{m'=1}^M \text{tr}((\tilde{\mathbf{W}}_{m,m'} \mathbf{p}_{XY})(\tilde{\mathbf{W}}_{m,m'} \mathbf{p}_{XY})^H + (\tilde{\mathbf{W}}_{m,m'} \mathbf{p}_X)(\tilde{\mathbf{W}}_{m,m'} \mathbf{p}_Y)^H),$$

where $\tilde{\mathbf{W}}_{m,m'} = \tilde{\mathbf{W}}_m \circ \tilde{\mathbf{W}}_{m'}^*.$

A proof is provided in Appendix A.

Remark 3.7. If $X = Y$, the results in Proposition 3.8 reduce to those of the windowed average periodogram in Marques et al. (2017).

Proposition 3.9. *Consider two windows \mathbf{w}_m and $\mathbf{w}_{m'}$ and assume that the distance between any node in the support of \mathbf{w}_m and any node in the support of $\mathbf{w}_{m'}$ is larger than $(L_1 + L_2)$ hops. If two processes X and Y are responses of graph filters \mathbf{H}_1 and \mathbf{H}_2 of degrees L_1 and L_2 to white inputs $\boldsymbol{\epsilon}_1$ and $\boldsymbol{\epsilon}_2$ such that $\text{Cov}(\boldsymbol{\epsilon}_1, \boldsymbol{\epsilon}_2) = \mathbf{I}$, then it holds that $\text{tr}((\tilde{\mathbf{W}}_{m,m'} \mathbf{p}_{XY})(\tilde{\mathbf{W}}_{m,m'} \mathbf{p}_{XY})^H) = 0$, where $\tilde{\mathbf{W}}_{m,m'} = \tilde{\mathbf{W}}_m \circ \tilde{\mathbf{W}}_{m'}^*.$*

A proof is described in Appendix A.

Remark 3.8. Proposition 3.9 plays an important role in window design. The MSE of $\hat{\mathbf{p}}_{XY}^{\mathcal{W}}$ is equal to the sum of squared bias and $\text{tr}(\text{Var}(\hat{\mathbf{p}}_{XY}^{\mathcal{W}}))$. From Proposition 3.8(b), $\text{tr}(\text{Var}(\hat{\mathbf{p}}_{XY}^{\mathcal{W}}))$ can be decomposed into two terms, one with $m = m'$ and the other with $m \neq m'$. The former term is $\frac{1}{M^2} \sum_{m=1}^M \text{tr}((\tilde{\mathbf{W}}_{m,m} \mathbf{p}_{XY})(\tilde{\mathbf{W}}_{m,m} \mathbf{p}_{XY})^H + (\tilde{\mathbf{W}}_{m,m} \mathbf{p}_X)(\tilde{\mathbf{W}}_{m,m} \mathbf{p}_Y)^H)$. By Proposition 3.7, it follows that $\text{tr}((\tilde{\mathbf{W}}_{m,m} \mathbf{p}_{XY})(\tilde{\mathbf{W}}_{m,m} \mathbf{p}_{XY})^H) = \|E(\hat{\mathbf{p}}_{XY}^{w_m})\|_2^2$. Given that $\|\mathbf{w}_m\|_2^2 = N$, it can be approximated by $\|\mathbf{p}_{XY}\|_2^2$. Similarly, we have $\text{tr}((\tilde{\mathbf{W}}_{m,m} \mathbf{p}_X)(\tilde{\mathbf{W}}_{m,m} \mathbf{p}_Y)^H) = \langle E(\hat{\mathbf{p}}_X^{w_m}), E(\hat{\mathbf{p}}_Y^{w_m}) \rangle$, which can be approximated by $\langle \mathbf{p}_X, \mathbf{p}_Y \rangle$. Thus, the former term is close to $\frac{1}{M} (\|\mathbf{p}_{XY}\|_2^2 + \langle \mathbf{p}_X, \mathbf{p}_Y \rangle) = \frac{1}{M} \text{tr}(\text{diag}(|\mathbf{p}_{XY}|^2) + \text{diag}(\mathbf{p}_X) \text{diag}(\mathbf{p}_Y))$. This implies that the latter term (when $m \neq m'$) contains the effect of the correlation between M windowed bivariate signals, referring to Proposition 3.6(b). Proposition 3.3 indicates that certain jointly weakly stationary graph processes exhibit localized cross-covariance structures. In this case, Proposition 3.9 suggests that designing non-overlapping windows can mitigate the effects of correlation between the windowed bivariate signals by reducing the latter term in the decomposition of $\text{Var}(\hat{\mathbf{p}}_{XY}^{\mathcal{W}})$. This leads to a reduction in the MSE of $\hat{\mathbf{p}}_{XY}^{\mathcal{W}}$. Moreover, according to Proposition 5 in Marques et al. (2017), if the distance between any node in the support of \mathbf{w}_m and any node in the support of $\mathbf{w}_{m'}$ is larger than $\max(L_1, L_2)$ hops, $\tilde{\mathbf{W}}_{m,m'} \mathbf{p}_X = \tilde{\mathbf{W}}_{m,m'} \mathbf{p}_Y = \mathbf{0}$. Therefore, if the distance between any node in the support of \mathbf{w}_m and any node in the support of $\mathbf{w}_{m'}$ is larger than $\max(2L_1, 2L_2)$ hops, the latter term in the decomposition of $\text{tr}(\text{Var}(\hat{\mathbf{p}}_{XY}^{\mathcal{W}}))$ becomes zero, which means that $\text{Var}(\hat{\mathbf{p}}_{XY}^{\mathcal{W}})$ behaves as if the windowed signals are independent.

3.4 Graph coherence

From the definitions of graph power spectral density and graph cross-spectral density, we define the graph coherence (or magnitude-squared graph coherence) between two jointly weakly stationary processes X and Y , denoted by \mathbf{c}_{XY} .

Definition 3.3. The coherence between zero-mean jointly weakly stationary graph processes X and Y is defined as $\mathbf{c}_{XY} = \frac{|\mathbf{p}_{XY}|^2}{\mathbf{p}_X \mathbf{p}_Y}$, where the product and division operators are applied elementwise.

Proposition 3.10. *The graph coherence satisfies the following inequality, $\mathbf{0} \leq \mathbf{c}_{XY} \leq \mathbf{1}$,*

where \leq indicates elementwise inequality. The equality $\mathbf{c}_{XY} = \mathbf{0}$ holds when X and Y are uncorrelated, and $\mathbf{c}_{XY} = \mathbf{1}$ holds when $Y = \mathbf{H}X$ for a filter \mathbf{H} .

A proof is given in Appendix A.

4 Practical implementation

4.1 Window design

Designing windows is crucial for the estimation performance of the windowed average graph cross-periodogram. Marques et al. (2017) addressed window design for the windowed average graph periodogram, but this remains a challenging and open problem. As suggested by Marques et al. (2017), for each window \mathbf{w}_m , $\tilde{\mathbf{W}}_m$ should be close to the identity matrix so that the windowed signal and the original signal are similar in the graph frequency domain. In this regard, we can adopt random windows that are close to the identity matrix. Also, as mentioned in Remark 3.8, if a community structure exists in the graph, we can design non-overlapping local windows corresponding to each community.

In this study, we use random windows for practical implementation in the numerical experiments in Section 5. Specifically, we generate $\tilde{\mathbf{W}}_m$ as an identity matrix with random Gaussian noise added for each element. Then, we obtain \mathbf{w}_m from $\text{diag}(\mathbf{V}\tilde{\mathbf{W}}_m\mathbf{V}^H)$. However, it is important to note that this is not an optimal design and tends to degrade performance, especially when the number of nodes is small. Thus, we consider an alternative estimator for implementation.

4.2 Alternative estimator for graph cross-spectral density

Perraudin and Vandergheynst (2017) provided a perspective on the PSD estimation of Bartlett’s and Welch’s methods in classical signal processing, interpreting them as the averaging over time of the squared coefficients derived from a windowed Fourier transform. Based on this insight, they proposed an estimator of GPSD using the windowed graph Fourier transform introduced by Shuman et al. (2016). Specifically, for a graph kernel g that is concentrated at the origin (e.g., $g(\lambda) = e^{-\lambda^2/\sigma^2}$ for a constant σ^2), g_k is defined by

shifting g as

$$g_k(\lambda_\ell) = g(\lambda_\ell - k\tau), \quad k = 1, \dots, K, \quad \tau = \frac{\lambda_{max}}{K}, \quad (4)$$

where λ_ℓ ($1 \leq \ell \leq N$) are the eigenvalues of \mathbf{S} and λ_{max} is the maximum value among them. Then, the windowed graph Fourier transform-based estimator is defined as

$$\hat{\mathbf{p}}_X^{WF}(k\tau) = \frac{\|g_k(\mathbf{S})\mathbf{x}\|_2^2}{\|g_k(\mathbf{S})\|_F^2} = \frac{\sum_{n=1}^N C_{n,k}^2}{\|g_k(\mathbf{S})\|_F^2}, \quad (5)$$

where $\|\cdot\|_F$ denotes the Frobenius norm, $g_k(\mathbf{S}) = \mathbf{V} \text{diag}(g_k(\lambda_\ell)) \mathbf{V}^H$, and $C_{n,k}$ denote the coefficients of the windowed graph Fourier transform, defined as

$$C_{n,k} = \langle \mathbf{x}, \mathcal{T}_n g_k \rangle = (g_k(\mathbf{S})\mathbf{x})_n.$$

Here, \mathcal{T}_n represents the localization operator such that $\mathcal{T}_n g = \sum_{\ell=1}^N g(\lambda_\ell) (\mathbf{v}_\ell^*)_n \mathbf{v}_\ell$, and $(\cdot)_n$ denotes the n th element operation on a vector.

Along the same line with the windowed graph Fourier transform-based estimator of GPSD in (5), we propose a windowed graph Fourier transform-based estimator of GCSD as

$$\hat{\mathbf{p}}_{XY}^{WF}(k\tau) = \frac{\langle g_k(\mathbf{S})\mathbf{x}, g_k(\mathbf{S})\mathbf{y} \rangle}{\|g_k(\mathbf{S})\|_F^2} = \frac{\sum_{n=1}^N \langle C_{n,k}^{(1)}, C_{n,k}^{(2)} \rangle}{\|g_k(\mathbf{S})\|_F^2}$$

for $k = 1, \dots, K$ and $\tau = \lambda_{max}/K$, where $C_{n,k}^{(1)} = \langle \mathbf{x}, \mathcal{T}_n g_k \rangle = (g_k(\mathbf{S})\mathbf{x})_n$ and $C_{n,k}^{(2)} = \langle \mathbf{y}, \mathcal{T}_n g_k \rangle = (g_k(\mathbf{S})\mathbf{y})_n$ for the localization operator \mathcal{T}_n and g_k defined in (4).

We remark that as noted in Perraudin and Vanderghelynst (2017), the difference between $\hat{\mathbf{p}}_{XY}^{WF}$ and the true GCSD \mathbf{p}_{XY} is insignificant when $\sigma \gg \lambda_{max}/N$. However, as σ decreases, the difference may increase.

We now investigate how the number of filters K affects the performance of the windowed graph Fourier transform-based estimator on the Minnesota road network, comprising 2642 nodes and 6606 edges, all with weights equal to 1, which is shown in the top left panel of Figure 5. Jointly weakly stationary graph processes are generated using \mathbf{H}_{ds} and \mathbf{H}_{high} with frequency responses defined as $\tilde{h}_{ds}(\lambda) = \sin(15\lambda)e^{-5\lambda}$ and $\tilde{h}_{high}(\lambda) = \lambda e^{-\lambda}$, respectively, resulting in the true GCSD being $\tilde{h}_{ds}(\lambda)\tilde{h}_{high}^*(\lambda)$. As in Section 3.3.1, we use

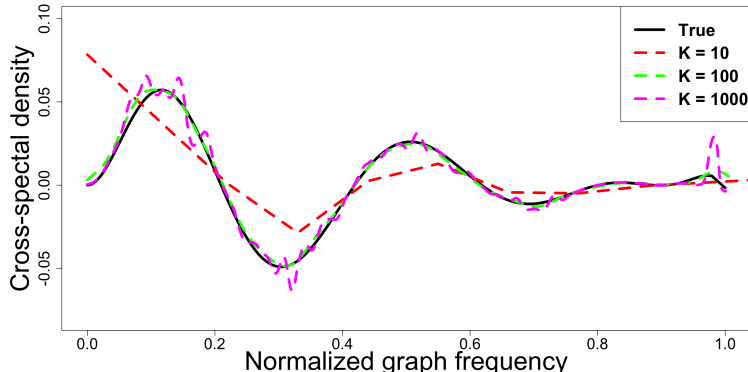


Figure 2: The windowed graph Fourier transform-based estimates for different values of K on the Minnesota road network.

the Chebyshev polynomial approximation and the graph Laplacian as a graph shift operator \mathcal{S} . Following Perraudin and Vandergheynst (2017), the graph kernel g is defined as $g(\lambda) = e^{-\lambda^2/\sigma^2}$, where σ^2 is chosen as $(K+1)\lambda_{max}/K^2$. The estimation results for the windowed graph Fourier transform-based estimators for different K 's are shown in Figure 2. As K increases, estimation performance improves. However, if K is too large, estimation becomes wiggly, and performance degrades. This is consistent with the discussion above about the effect of σ on estimation performance.

5 Numerical experiments

5.1 Detection of shared components

In this section, we demonstrate the importance of cross-spectral analysis on graphs by investigating the graph cross-periodogram for different irregular graphs. In particular, we generate two graph signals that share the same frequency, which is indistinguishable from the graph periodogram of each signal. However, in the cross-spectral analysis, this frequency can be revealed by the graph cross-periodogram.

We consider three irregular graphs: the Seoul Metropolitan railroad network, a random sensor network, and the Minnesota road network. In all scenarios, we compute the estimators of GPSD and GCSD using both windowed averaging and windowed graph

Fourier-based methods. Here, the graph Laplacian serves as a graph shift operator. For the window averaging approach, we utilize random windows as described in Section 4.1, appropriately choosing the number of windows M . For the windowed graph Fourier-based approach, we use the same graph kernel g in Section 4.2. The number of filters K is chosen to ensure that σ is significantly greater than λ_{max}/N , while still being large enough considering the number of nodes.

We first consider the Seoul railroad network studied by Kim and Oh (2024). This network has 243 stations as nodes and is connected by railroads. The edge weight between the i th node and the j th node is determined by $w_{ij} = \exp(-d^2(i, j)/ave^2)$, where $d(i, j)$ represents the distance between the i th and j th nodes computed by summing the lengths of the railroads connecting the two nodes, and ave denotes the average distance between the nodes. We generate two signals as $\mathbf{x}_{metro} = 5\mathbf{v}_{100}^{metro} + 100\mathbf{v}_{50}^{metro}$ and $\mathbf{y}_{metro} = 5\mathbf{v}_{100}^{metro} + 100\mathbf{v}_{150}^{metro}$, where \mathbf{v}_i^{metro} denotes the i th eigenvector of the graph Laplacian, corresponding to the i th eigenvalue λ_i^{metro} . Figure 3 shows that \mathbf{x}_{metro} predominantly contains \mathbf{v}_{50}^{metro} , while \mathbf{y}_{metro} primarily consists of \mathbf{v}_{150}^{metro} . This reasoning is consistent with what we observed in the graph periodograms of the two signals, as shown in Figures 6 and 7. For each estimator, the values of M and K are set to 100, respectively. However, based on these results, we cannot discern the shared component \mathbf{v}_{100}^{metro} between the two signals; this identification becomes feasible through cross-spectral analysis. The GPSD estimates in Figures 6 and 7 show peaks at the graph frequency corresponding roughly to λ_{100}^{metro} . These observations indicate that the two signals share the component \mathbf{v}_{100}^{metro} .

Next, we conduct a similar analysis on a random sensor network shown in the top left panel of Figure 4. The random sensor network is constructed by randomly selecting 400 nodes located in $[0, 20] \times [0, 20]$, where the x - and y -coordinates are independently generated from a uniform distribution $\mathcal{U}(0, 20)$. Each node is then connected to its five nearest neighbors. The edge weights are determined in the same way as the Seoul Metropolitan railroad network, where the distance represents the Euclidean distance. Two signals are generated as $\mathbf{x}_{rsn} = 5\mathbf{v}_{300}^{rsn} + 100\mathbf{v}_{100}^{rsn}$ and $\mathbf{y}_{rsn} = 5\mathbf{v}_{300}^{rsn} + 100\mathbf{v}_{200}^{rsn}$, where \mathbf{v}_i^{rsn} denotes the i th eigenvector of the graph Laplacian, corresponding to the i th eigenvalue λ_i^{rsn} . The common component between the two signals, \mathbf{v}_{300}^{rsn} , is uncovered in the GCSF estimates with

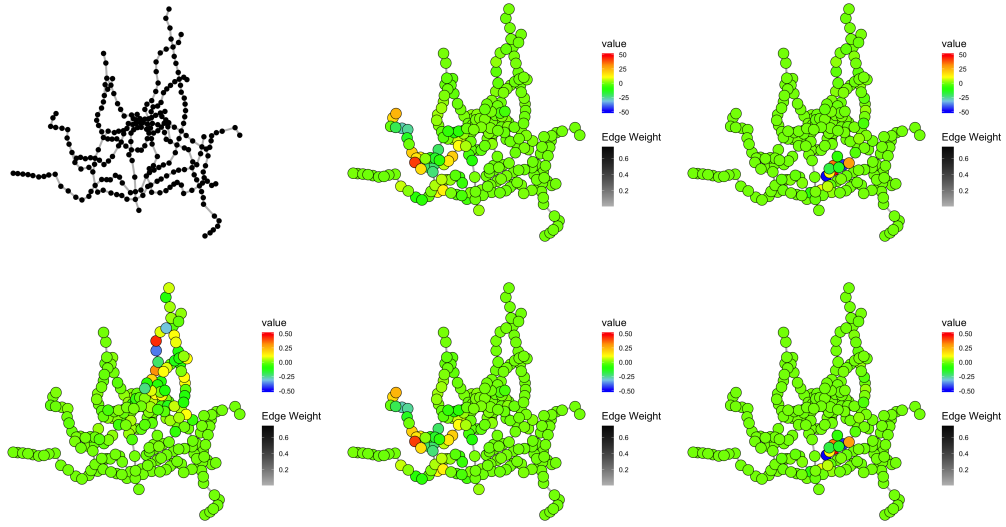


Figure 3: Visualization of the Seoul Metropolitan railroad network and signals: Seoul Metropolitan railroad network (top left), $\mathbf{x}_{\text{metro}}$ (top center), $\mathbf{y}_{\text{metro}}$ (top right), $\mathbf{v}_{100}^{\text{metro}}$ (bottom left), $\mathbf{v}_{50}^{\text{metro}}$ (bottom center), $\mathbf{v}_{150}^{\text{metro}}$ (bottom right).

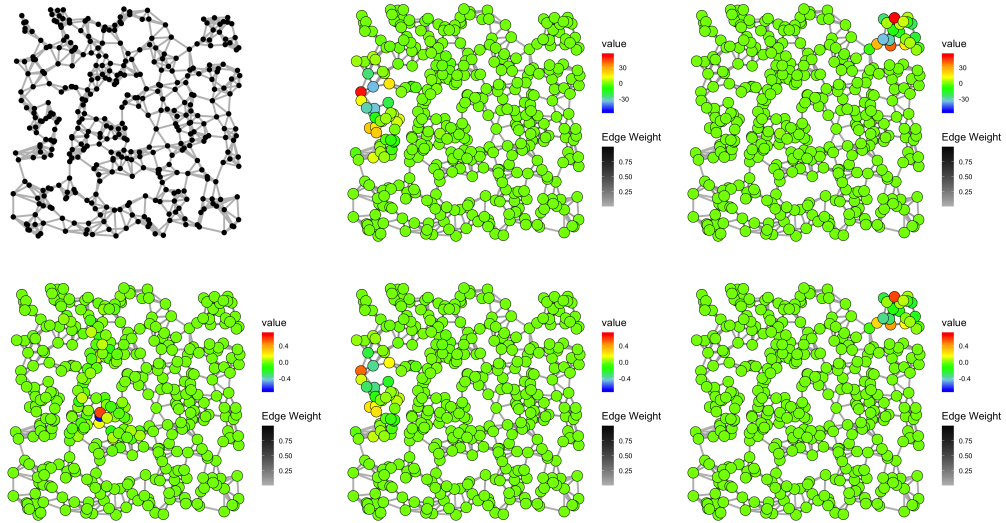


Figure 4: Visualization of a random sensor network and signals: random sensor network (top left), \mathbf{x}_{rsn} (top center), \mathbf{y}_{rsn} (top right), $\mathbf{v}_{300}^{\text{rsn}}$ (bottom left), $\mathbf{v}_{100}^{\text{rsn}}$ (bottom center), $\mathbf{v}_{200}^{\text{rsn}}$ (bottom right).

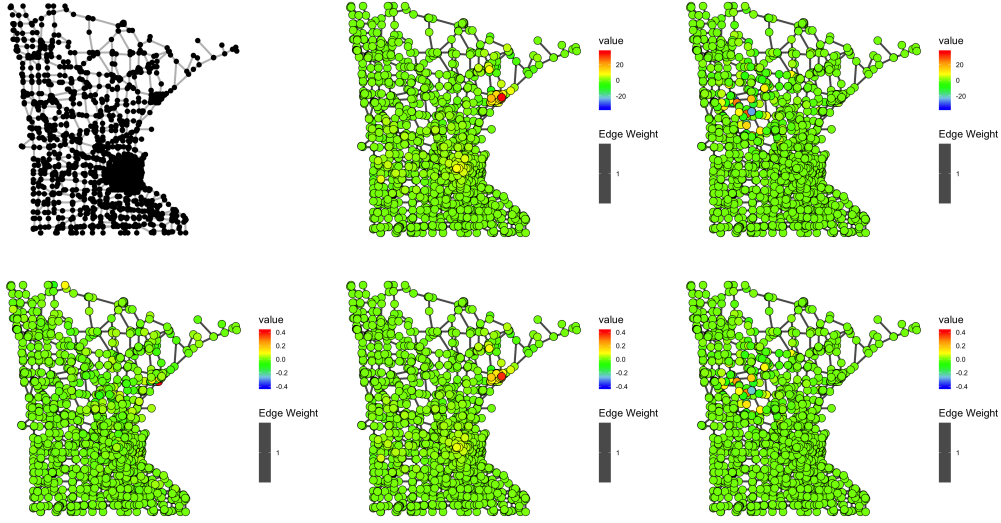


Figure 5: Visualization of the Minnesota road network and signals: Minnesota road network (top left), $\mathbf{x}_{\text{minne}}$ (top center), $\mathbf{y}_{\text{minne}}$ (top right), $\mathbf{v}_{500}^{\text{minne}}$ (bottom left), $\mathbf{v}_{1000}^{\text{minne}}$ (bottom center), $\mathbf{v}_{2000}^{\text{minne}}$ (bottom right).

$M = 100$ and $K = 50$, as shown in Figures 6 and 7.

Finally, we use the Minnesota road network for analysis. We generate two signals as $\mathbf{x}_{\text{minne}} = 5\mathbf{v}_{500}^{\text{minne}} + 100\mathbf{v}_{1000}^{\text{minne}}$ and $\mathbf{y}_{\text{minne}} = 5\mathbf{v}_{500}^{\text{minne}} + 100\mathbf{v}_{2000}^{\text{minne}}$. Here, $\mathbf{v}_i^{\text{minne}}$ denotes the i th eigenvector of the graph Laplacian, corresponding to the i th eigenvalue λ_i^{minne} . The GCSD estimates obtained with $M = 100$ and $K = 100$ reveal the common component between the two signals, $\mathbf{v}_{500}^{\text{minne}}$, as shown in Figures 6 and 7.

5.2 Cross-spectral analysis on meteorological dataset

We apply the proposed cross-spectral analysis method to a meteorological dataset collected hourly during January 2014 in Brest, France. The dataset contains temperature and humidity measurements recorded at 22 weather stations. The original data are available at <https://donneespubliques.meteofrance.fr>. To construct the graph, each node is connected to its six nearest neighbors, and the edge weights are determined in the same manner as the random sensor network used in Section 5.1. When calculating the distance between two nodes, we use the weighted 3D coordinates of each station as suggested by Perraudin and Vandergheynst (2017), where we multiply the z -coordinate by 5 since the

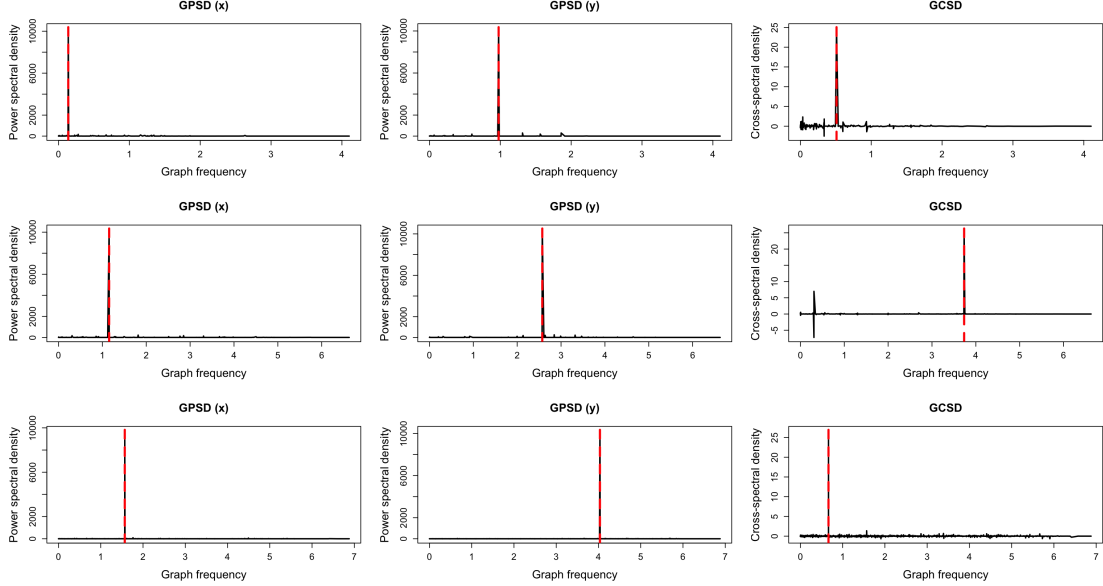


Figure 6: Cross-spectral analysis results on three networks: Seoul Metropolitan railroad network (top row), random sensor network (middle row), and Minnesota road network (bottom row). Each column, from left to right, illustrates the windowed average estimates of GPSD of X , Y , and GCSD, respectively.

elevation is considered more important than other coordinates. The resultant graph is shown in Figure 9. We average the hourly data to obtain the monthly average temperature and humidity for January. Subsequently, we subtract the mean signals across nodes to ensure that they are observations from zero-mean processes. For the graph shift operator, we use the graph Laplacian whose i th eigenvector corresponding to the i th eigenvalue λ_i^{brest} is denoted by $\mathbf{v}_i^{\text{brest}}$. Since the graph has few nodes, we estimate GPSD and GCSD using the windowed graph Fourier transform-based estimator with the same graph kernel g as in the previous section. The number of filters K is set to 40.

Figure 8 shows the estimation results. The GPSD estimates for temperature and humidity peak at 0.714 and 2.142, aligning closely with λ_3^{brest} and λ_7^{brest} . This suggests that the temperature exhibits a predominant pattern associated with $\mathbf{v}_3^{\text{brest}}$, while the humidity follows a predominant pattern linked to $\mathbf{v}_7^{\text{brest}}$. As shown in Figure 9, this observation is plausible. Cross-spectral analysis provides additional insights into the relationship between two measurements. The negative peaks of 0.714 and 2.142 in the GCSD estimate

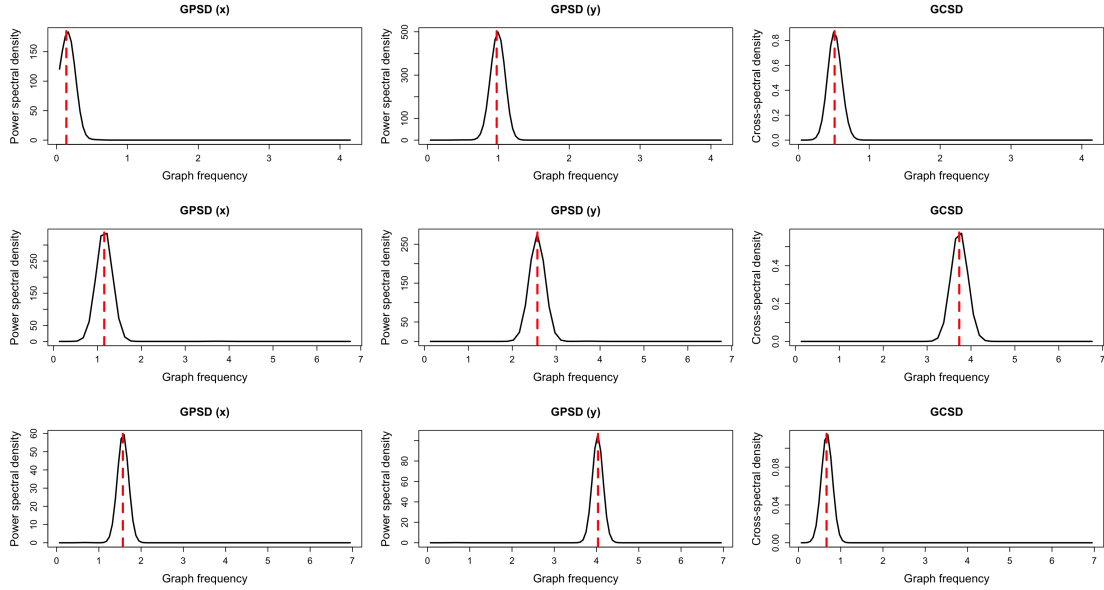


Figure 7: Cross-spectral analysis results on three networks: Seoul Metropolitan railroad network (top row), random sensor network (middle row), and Minnesota road network (bottom row). Each column, from left to right, illustrates the windowed graph Fourier transform-based estimates of GPSD of X , Y , and GCSD, respectively.

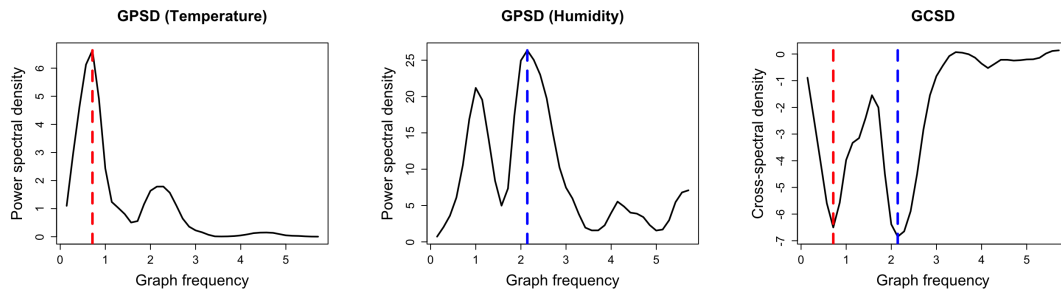


Figure 8: Cross-spectral analysis results on the Brest meteorological dataset: windowed graph Fourier transform-based estimates of GPSD for temperature (left), humidity (middle), and GCSD (right).

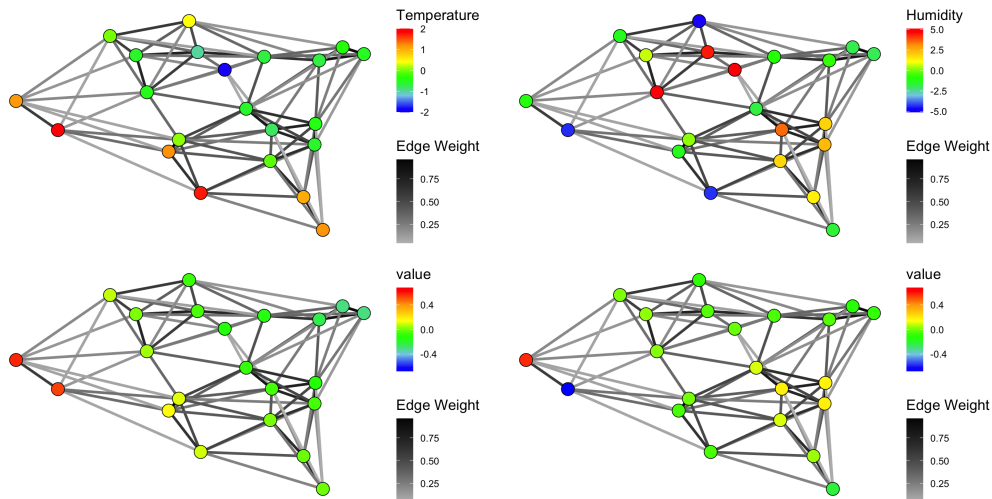


Figure 9: Visualization of signals on the Brest weather network: centered monthly average temperature for January (top left), centered monthly average humidity for January (top right), $\mathbf{v}_3^{\text{brest}}$ (bottom left), and $\mathbf{v}_7^{\text{brest}}$ (bottom right).

imply that temperature and humidity share two primary components, $\mathbf{v}_3^{\text{brest}}$ and $\mathbf{v}_7^{\text{brest}}$, respectively, with opposite signs. This is consistent with a simple visual inspection plotting temperature and humidity across node index, which shows the opposite behavioral trends.

6 Robust spectral analysis on graphs

In this section, we discuss robust spectral analysis on graphs, proposing M -type estimators of GPSD and GCSD. It is natural to robustify the graph periodogram and the windowed average graph periodogram by utilizing the Huber loss function ρ_c (Huber, 1964) as

$$\rho_c(t) = \begin{cases} t^2 & \text{if } |t| \leq c, \\ 2c(|t| - c/2) & \text{if } |t| > c, \end{cases}$$

for a cutoff constant $c > 0$. By replacing L_2 loss in (1) with the Huber loss, an M -type estimator $\hat{\mathbf{p}}_{X,c}$ of GPSD can be defined as

$$\hat{\mathbf{p}}_{X,c} = \arg \min_{\mathbf{p}} \sum_{i=1}^{N^2} \rho_c((\hat{\boldsymbol{\sigma}}_X - \mathbf{G}\mathbf{p})_i).$$

In addition, the windowed average graph periodogram can be considered as a least squares solution. To be specific, for $\mathbf{x}_{\mathbf{w}_m} := \text{diag}(\mathbf{w}_m)\mathbf{x}$, $\hat{\mathbf{p}}_X^{\mathcal{W}}$ of (2) is equal to $\frac{1}{M} \sum_{m=1}^M |\mathbf{V}^H \mathbf{x}_{\mathbf{w}_m}|^2$; thus, it is a least squares solution of \mathbf{p} that minimizes $\|\hat{\boldsymbol{\sigma}}_X^{\mathcal{W}} - \mathbf{G}\mathbf{p}\|_2^2$, where $\hat{\boldsymbol{\sigma}}_X^{\mathcal{W}} = \text{vec}(\hat{\boldsymbol{\Sigma}}_X^{\mathcal{W}})$ and $\hat{\boldsymbol{\Sigma}}_X^{\mathcal{W}} = \frac{1}{M} \sum_{m=1}^M \mathbf{x}_{\mathbf{w}_m} \mathbf{x}_{\mathbf{w}_m}^H$. Here, $\mathbf{x}_{\mathbf{w}_m} := \text{diag}(\mathbf{w}_m)\mathbf{x}$ and $\mathbf{y}_{\mathbf{w}_m} := \text{diag}(\mathbf{w}_m)\mathbf{y}$. Therefore, we define an M -type estimator of GPSD as

$$\hat{\mathbf{p}}_{X,c}^{\mathcal{W}} = \arg \min_{\mathbf{p}} \sum_{i=1}^{N^2} \rho_c((\hat{\boldsymbol{\sigma}}_X^{\mathcal{W}} - \mathbf{G}\mathbf{p})_i).$$

Similarly, we obtain a robust graph cross-periodogram as

$$\hat{\mathbf{p}}_{XY,c} = \arg \min_{\mathbf{p}} \sum_{i=1}^{N^2} \rho_c((\hat{\boldsymbol{\sigma}}_{XY} - \mathbf{G}\mathbf{p})_i).$$

We also define an M -type estimator by modifying the windowed average graph cross-periodogram as

$$\hat{\mathbf{p}}_{XY,c}^{\mathcal{W}} = \arg \min_{\mathbf{p}} \sum_{i=1}^{N^2} \rho_c((\hat{\boldsymbol{\sigma}}_{XY}^{\mathcal{W}} - \mathbf{G}\mathbf{p})_i),$$

where $\hat{\boldsymbol{\sigma}}_{XY}^{\mathcal{W}} = \text{vec}(\hat{\boldsymbol{\Sigma}}_{XY}^{\mathcal{W}})$ and $\hat{\boldsymbol{\Sigma}}_{XY}^{\mathcal{W}} = \sum_{m=1}^M \mathbf{x}_{\mathbf{w}_m} \mathbf{y}_{\mathbf{w}_m}^H$.

We demonstrate the robustness of the proposed M -type windowed average graph periodogram and M -type windowed average graph cross-periodogram by simulating signals with outliers on the Karate club network. We compare M -type windowed average estimators with the original windowed average estimators. We use the graph Laplacian as the graph shift operator and utilize 100 random windows. When calculating M -type windowed average estimators, we use the Huber loss function ρ_c with $c = 0.25$, and the optimization solution is computed using the iteratively reweighted least squares method.

The left panel of Figure 10 shows the robustness of the M -type windowed average graph periodogram compared to the original windowed average graph periodogram. The signal is generated as $\mathbf{x}_{\text{karate}} = 3\mathbf{v}_{20}^{\text{karate}}$, where $\mathbf{v}_i^{\text{karate}}$ denotes the i th eigenvector of the graph Laplacian corresponding to the i th eigenvalue $\lambda_i^{\text{karate}}$. A signal with an outlier is obtained by setting the signal value of the 25th node to 4, which is greater than the maximum signal value of the original signal. As expected, the windowed average graph

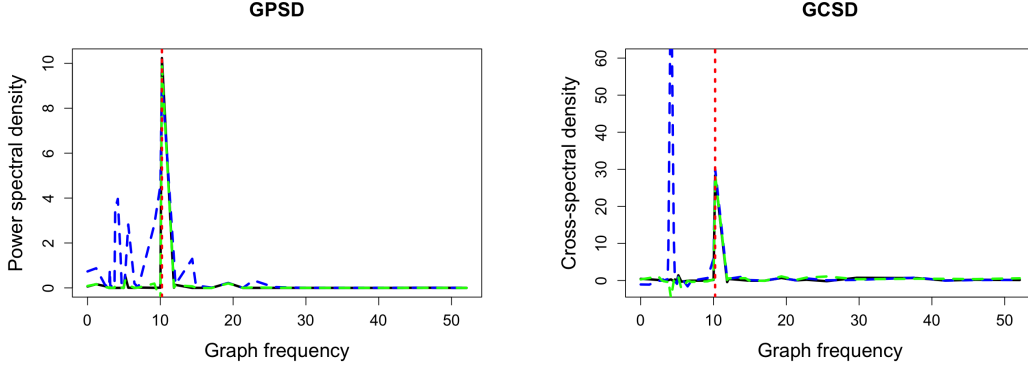


Figure 10: Estimation results with outliers: GPSD estimation (left) and GCSD estimation (right). The windowed average estimate using data without outliers (black), the estimate using data with outliers (blue dashed), the M -type windowed average estimate using data with outliers (green dashed), and frequency corresponding to $\lambda_{20}^{\text{karate}}$ (red dotted).

periodogram peaks at $\lambda_{20}^{\text{karate}}$ when computed using the data without outliers, but the estimates become inaccurate when calculated using the data with outliers. On the other hand, the M -type windowed average estimate is robust to the outlier, closely resembling the results of the windowed average graph periodogram obtained from the data without outliers.

We now evaluate the robustness of the M -type windowed average graph cross-periodogram. To this end, we generate two signals as $\mathbf{x}_{\text{karate}} = 5\mathbf{v}_{20}^{\text{karate}} + 20\mathbf{v}_{30}^{\text{karate}}$ and $\mathbf{y}_{\text{karate}} = 5\mathbf{v}_{20}^{\text{karate}} + 20\mathbf{v}_{10}^{\text{karate}}$. Signals with outliers are obtained by setting the signal value of $\mathbf{x}_{\text{karate}}$ at the 25th node to -10 and the signal value of $\mathbf{y}_{\text{karate}}$ at the 15th node to 10, respectively. The right panel of Figure 10 shows the robustness of the M -type windowed average graph cross-periodogram. As one can see, the M -type windowed average estimate correctly captures the common graph frequency $\lambda_{20}^{\text{karate}}$ between the two signals.

We leave the theoretical properties of the M -type estimators to future research.

7 Concluding remarks

In this study, we explored cross-spectral analysis tools for graph signals. We defined concepts such as joint weak stationarity, cross-spectral density, and coherence on graphs. We

proposed several estimators for graph cross-spectral density and provided theoretical properties related to the definitions and estimators. Through numerical experiments on various irregular graphs, we investigated the usefulness and performance of these estimators. The results demonstrated the effectiveness of cross-spectral analysis in identifying shared behaviors between two graph processes that cannot be easily achieved solely through visualization or spectral analysis of a single graph process. We further suggested robustifying the proposed estimators to make them robust to outliers. This work contributes to the emerging field of multivariate graph signal processing, which has yet to be extensively studied.

There are several avenues for further development in this area. First, designing optimal windows for evaluating the windowed average graph cross-periodograms remains an open question. The study of non-stationary graph processes also presents an opportunity for further research. Locally stationary graph processes introduced by Canbolat and Vural (2024) can be a promising starting point. Furthermore, the development of a wavelet-based graph periodogram or graph cross-periodogram for such processes can be pursued in future work. These approaches have the potential to advance our understanding of graph signal processing and are left as future work.

Acknowledgments

This research was supported by the National Research Foundation of Korea (NRF) funded by the Korea government (2021R1A2C1091357).

Appendix A Proofs

A.1 Proof of Proposition 3.1

Proof. We follow similar processes of proofs outlined in Marques et al. (2017). The equivalence between Definition 3.1(b) and (c) can be readily demonstrated by following the proof provided in Marques et al. (2017). To prove the equivalence between Definition 3.1(a) and (c), let us first assume that Definition 3.1(a) holds. Given $\mathbf{S} = \mathbf{V}\mathbf{\Lambda}\mathbf{V}^H$, let us define $\tilde{\mathbf{h}}_i := \text{diag}(\sum_{\ell=0}^{N-1} h_{i,\ell}\mathbf{S}^\ell)$ and $\mathbf{h}_i := (h_{i,0}, \dots, h_{i,N-1})^\top$ ($i = 1, 2$). We further let $\lambda_j = (\mathbf{\Lambda})_{j,j}$ and $\mathbf{\Psi}$ be the $N \times N$ Vandermonde matrix with entries $\psi_{jk} = \lambda_j^{k-1}$. Then, we can rewrite \mathbf{H}_i ($i = 1, 2$) as

$$\mathbf{H}_i = \sum_{\ell=0}^{N-1} h_{i,\ell}\mathbf{S}^\ell = \mathbf{V} \text{diag}(\tilde{\mathbf{h}}_i)\mathbf{V}^H = \mathbf{V} \text{diag}(\mathbf{\Psi}\mathbf{h}_i)\mathbf{V}^H.$$

Consequently, by letting $\mathbf{V}^H \text{Cov}(\boldsymbol{\epsilon}_1, \boldsymbol{\epsilon}_2)\mathbf{V} = \text{diag}(\tilde{\boldsymbol{\epsilon}})$,

$$\begin{aligned} \boldsymbol{\Sigma}_X &= E\left((\mathbf{H}_1\boldsymbol{\epsilon}_1)(\mathbf{H}_1\boldsymbol{\epsilon}_1)^H\right) = \mathbf{H}_1 E(\boldsymbol{\epsilon}_1\boldsymbol{\epsilon}_1^H)\mathbf{H}_1^H = \mathbf{H}_1\mathbf{H}_1^H = \mathbf{V} \text{diag}(|\tilde{\mathbf{h}}_1|^2)\mathbf{V}^H, \\ \boldsymbol{\Sigma}_Y &= E\left((\mathbf{H}_2\boldsymbol{\epsilon}_2)(\mathbf{H}_2\boldsymbol{\epsilon}_2)^H\right) = \mathbf{H}_2 E(\boldsymbol{\epsilon}_2\boldsymbol{\epsilon}_2^H)\mathbf{H}_2^H = \mathbf{H}_2\mathbf{H}_2^H = \mathbf{V} \text{diag}(|\tilde{\mathbf{h}}_2|^2)\mathbf{V}^H, \\ \boldsymbol{\Sigma}_{XY} &= E\left((\mathbf{H}_1\boldsymbol{\epsilon}_1)(\mathbf{H}_2\boldsymbol{\epsilon}_2)^H\right) = \mathbf{H}_1 E(\boldsymbol{\epsilon}_1\boldsymbol{\epsilon}_2^H)\mathbf{H}_2^H = \mathbf{V} \text{diag}(\tilde{\boldsymbol{\gamma}})\mathbf{V}^H, \end{aligned}$$

where $\tilde{\boldsymbol{\gamma}} = \tilde{\mathbf{h}}_1 \circ \tilde{\boldsymbol{\epsilon}} \circ \tilde{\mathbf{h}}_2^*$. This leads to Definition 3.1(c). Conversely, if Definition 3.1(c) holds, there exist $N \times 1$ vectors $\tilde{\boldsymbol{\gamma}}_1$, $\tilde{\boldsymbol{\gamma}}_2$, and $\tilde{\boldsymbol{\gamma}}_{12}$ satisfying $\boldsymbol{\Sigma}_X = \mathbf{V} \text{diag}(\tilde{\boldsymbol{\gamma}}_1)\mathbf{V}^H$, $\boldsymbol{\Sigma}_Y = \mathbf{V} \text{diag}(\tilde{\boldsymbol{\gamma}}_2)\mathbf{V}^H$, and $\boldsymbol{\Sigma}_{XY} = \mathbf{V} \text{diag}(\tilde{\boldsymbol{\gamma}}_{12})\mathbf{V}^H$. Here, $\tilde{\boldsymbol{\gamma}}_1$ and $\tilde{\boldsymbol{\gamma}}_2$ are elementwise nonnegative vectors because $\boldsymbol{\Sigma}_X$ and $\boldsymbol{\Sigma}_Y$ are positive semi-definite matrices. Since the eigenvalues of \mathbf{S} are all distinct and $\mathbf{\Psi}$ is a full rank $N \times N$ Vandermonde matrix, there exist unique solutions \mathbf{h}_1 and \mathbf{h}_2 satisfying $\mathbf{\Psi}\mathbf{h}_1 = \sqrt{\tilde{\boldsymbol{\gamma}}_1}$ and $\mathbf{\Psi}\mathbf{h}_2 = \sqrt{\tilde{\boldsymbol{\gamma}}_2}$, where the square root is applied elementwise. Then, by choosing $\tilde{\boldsymbol{\epsilon}}$ to satisfy $\tilde{\boldsymbol{\epsilon}} = \frac{\tilde{\boldsymbol{\gamma}}_{12}}{\sqrt{\tilde{\boldsymbol{\gamma}}_1} \circ \sqrt{\tilde{\boldsymbol{\gamma}}_2}}$, Definition 3.1(a) holds. \square

A.2 Proof of Proposition 3.2

Proof. We have $\mathbf{H}_i = \mathbf{V} \text{diag}(\tilde{\mathbf{h}}_i) \mathbf{V}^H$ ($i = 1, 2$) and $\boldsymbol{\Sigma}_{XY} = \mathbf{V} \text{diag}(\mathbf{p}_{XY}) \mathbf{V}^H$. By using these three equations, we can derive

$$\boldsymbol{\Sigma}_{ZW} = \mathbf{H}_1 \boldsymbol{\Sigma}_{XY} \mathbf{H}_2^H = \mathbf{V} \text{diag}(\tilde{\mathbf{h}}_1) \text{diag}(\mathbf{p}_{XY}) \text{diag}(\tilde{\mathbf{h}}_2^*) \mathbf{V}^H.$$

It completes the proofs for (a) and (b). \square

A.3 Proof of Proposition 3.3

Proof. Since \mathbf{H}_1 and \mathbf{H}_2 are linear shift-invariant, by Sandryhaila and Moura (2013a), we can rewrite \mathbf{H}_1 and \mathbf{H}_2 as

$$\mathbf{H}_i = \sum_{\ell=0}^{L_i-1} h_{i,\ell} \mathbf{S}^\ell, \quad i = 1, 2.$$

Since $S_{i,j}$ is nonzero only if $i = j$ or the i th node and the j th node are connected, it is clear that $(\mathbf{S}^\ell)_{i,j}$ is nonzero only if the distance between the i th node and the j th node is equal to or less than ℓ . Based on the fact that $\boldsymbol{\Sigma}_{XY} = \mathbf{H}_1 \mathbf{H}_2^H$, and that it is a polynomial of \mathbf{S} and \mathbf{S}^H of order $L_1 + L_2 - 2$, the proof is completed. \square

A.4 Proof of Proposition 3.4

Proof. We can compute the covariance matrix of \tilde{X} as follows, and the proof is completed.

$$\boldsymbol{\Sigma}_{\tilde{X}\tilde{Y}} = E(\tilde{X}\tilde{Y}^H) = \mathbf{V}^H E(XY^H) \mathbf{V} = \mathbf{V}^H \boldsymbol{\Sigma}_{XY} \mathbf{V} = \text{diag}(\mathbf{p}_{XY}).$$

\square

A.5 Proof of Proposition 3.5

Proof. Denote the i th column and the (i, j) th element of the matrix \mathbf{V} by \mathbf{v}_i and v_{ij} , respectively. We show that the i th element of $\hat{\mathbf{p}}_{XY}^p$ is equal to that of $\hat{\mathbf{p}}_{XY}^c$ as

$$(\hat{\mathbf{p}}_{XY}^c)_i = \left(\mathbf{V}^H \left(\frac{1}{R} \sum_{r=1}^R \mathbf{x}_r \mathbf{y}_r^H \right) \mathbf{V} \right)_{i,i} = \frac{1}{R} \sum_{r=1}^R \mathbf{v}_i^H \mathbf{x}_r \mathbf{y}_r^H \mathbf{v}_i = \frac{1}{R} \sum_{r=1}^R (\mathbf{v}_i^H \mathbf{x}_r) (\mathbf{v}_i^H \mathbf{y}_r)^* = (\hat{\mathbf{p}}_{XY}^p)_i.$$

Therefore, $\hat{\mathbf{p}}_{XY}^p = \hat{\mathbf{p}}_{XY}^c$. Now, we show that the i th element of $\hat{\mathbf{p}}_{XY}^c$ is equal to that of $\hat{\mathbf{p}}_{XY}^{ls}$. It can be easily shown that $\mathbf{G}^H \mathbf{G} = \mathbf{I}$. Thus, $\hat{\mathbf{p}}_{XY}^{ls} = \mathbf{G}^H \hat{\boldsymbol{\sigma}}_{XY}$. Then,

$$(\hat{\mathbf{p}}_{XY}^{ls})_i = (\mathbf{G}^H \hat{\boldsymbol{\sigma}}_{XY})_i = (v_{i1} \mathbf{v}_i^H, \dots, v_{iN} \mathbf{v}_i^H) \hat{\boldsymbol{\sigma}}_{XY} = \mathbf{v}_i^H \hat{\boldsymbol{\Sigma}}_{XY} \mathbf{v}_i = (\hat{\mathbf{p}}_{XY}^c)_i.$$

Hence, $\hat{\mathbf{p}}_{XY}^c = \hat{\mathbf{p}}_{XY}^{ls}$. The proof is completed. \square

A.6 Proof of Proposition 3.6

To prove Proposition 3.6, we first present and prove several lemmas and theorems.

Lemma A.1. (*Isserlis' Theorem, Isserlis, 1918*)

If $(Z_1, \dots, Z_n)^\top$ is a zero-mean real (or complex)-valued multivariate normal random vector, then the expectation of the product of random vector elements can be computed as

$$E(Z_1 Z_2 \cdots Z_n) = \sum_{P \in \mathbb{P}_n} \prod_{\{i,j\} \in P} E(Z_i Z_j),$$

where \mathbb{P}_n is the set of all distinct ways of partitioning $\{1, \dots, n\}$ into pairs. Specifically, $\mathbb{P}_n = \{\{P_1, \dots, P_{n/2}\} \mid P_1, \dots, P_{n/2} \text{ are disjoint sets, each containing two elements, and } P_1 \cup \dots \cup P_{n/2} = \{1, \dots, n\}\}$ if n is even; otherwise, \mathbb{P}_n is an empty set.

Proof. Refer to Isserlis (1918). \square

Lemma A.2. Let \mathbf{u} and \mathbf{v} be real-valued multivariate normal random vectors with $\mathbf{u} \sim N(\mathbf{0}, \boldsymbol{\Sigma}_{\mathbf{u}})$, $\mathbf{v} \sim N(\mathbf{0}, \boldsymbol{\Sigma}_{\mathbf{v}})$ and $\text{Cov}(\mathbf{u}, \mathbf{v}) = \boldsymbol{\Sigma}_{\mathbf{uv}}$. For real (or complex) matrices $\mathbf{A}, \mathbf{B}, \mathbf{C}, \mathbf{D}$, and real (or complex) vectors $\mathbf{a}, \mathbf{b}, \mathbf{c}, \mathbf{d}$, the following equation holds.

$$E(\mathbf{A} \mathbf{u} \mathbf{v}^\top \mathbf{B}^\top \mathbf{C} \mathbf{u} \mathbf{v}^\top \mathbf{D}^\top) = \mathbf{A} \boldsymbol{\Sigma}_{\mathbf{uv}} \mathbf{B}^\top \mathbf{C} \boldsymbol{\Sigma}_{\mathbf{uv}} \mathbf{D}^\top + \mathbf{A} \boldsymbol{\Sigma}_{\mathbf{u}} \mathbf{C}^\top \mathbf{B} \boldsymbol{\Sigma}_{\mathbf{v}} \mathbf{D}^\top + \mathbf{A} \boldsymbol{\Sigma}_{\mathbf{uv}} \mathbf{D}^\top \text{tr}(\mathbf{B}^\top \mathbf{C} \boldsymbol{\Sigma}_{\mathbf{uv}}).$$

Proof. It is sufficient to show that the $(1, 1)$ th element of both sides of the equation are equal. Denote the i th rows of $\mathbf{A}, \mathbf{B}, \mathbf{C}, \mathbf{D}$ by $\mathbf{A}_i^\top, \mathbf{B}_i^\top, \mathbf{C}_i^\top, \mathbf{D}_i^\top$, respectively, and the i th element of $\mathbf{A} \mathbf{u}, \mathbf{B} \mathbf{v}, \mathbf{C} \mathbf{u}, \mathbf{D} \mathbf{v}$ by a_i, b_i, c_i, d_i , respectively. Additionally, let $\mathbf{w} = (\mathbf{u}^\top, \mathbf{v}^\top)^\top$.

Then, the (1,1)th element of the left-hand side becomes $\sum_{i=1}^n a_1 b_i c_i d_1$. We note that

$$(a_1, b_i, c_i, d_1)^\top = \begin{pmatrix} \frac{\mathbf{A}_1^\top \mathbf{0}^\top}{\mathbf{0}^\top \mathbf{B}_i^\top} \\ \frac{\mathbf{C}_i^\top \mathbf{0}^\top}{\mathbf{0}^\top \mathbf{D}_1^\top} \end{pmatrix} \mathbf{w} \sim N(\mathbf{0}, \cdot).$$

Thus, by Lemma A.1, $E(a_1 b_i c_i d_1) = E(a_1 b_i)E(c_i d_1) + E(a_1 c_i)E(b_i d_1) + E(a_1 d_1)E(b_i c_i)$. The summation of the first term in the right-hand side over i , $\sum_{i=1}^n E(a_1 b_i)E(c_i d_1)$, becomes the (1,1)th element of $E(\mathbf{A}\mathbf{u}\mathbf{v}^\top \mathbf{B}^\top)E(\mathbf{C}\mathbf{u}\mathbf{v}^\top \mathbf{D}^\top)$, which is equal to the (1,1)th element of $\mathbf{A}\boldsymbol{\Sigma}_{\mathbf{u}\mathbf{v}}\mathbf{B}^\top \mathbf{C}\boldsymbol{\Sigma}_{\mathbf{u}\mathbf{v}}\mathbf{D}^\top$. Similarly, $\sum_{i=1}^n E(a_1 c_i)E(b_i d_1)$ is equal to the (1,1)th element of $\mathbf{A}\boldsymbol{\Sigma}_{\mathbf{u}}\mathbf{C}^\top \mathbf{B}\boldsymbol{\Sigma}_{\mathbf{v}}\mathbf{D}^\top$. Finally, $\sum_{i=1}^n E(a_1 d_1)E(b_i c_i) = E(a_1 d_1) \sum_{i=1}^n E(b_i c_i)$ is equal to the (1,1)th element of $E(\mathbf{A}\mathbf{u}\mathbf{v}^\top \mathbf{D}^\top)E(\mathbf{v}^\top \mathbf{B}^\top \mathbf{C}\mathbf{u})$, which is equal to the (1,1)th element of $\mathbf{A}\boldsymbol{\Sigma}_{\mathbf{u}\mathbf{v}}\mathbf{D}^\top \text{tr}(\mathbf{B}^\top \mathbf{C}\boldsymbol{\Sigma}_{\mathbf{u}\mathbf{v}})$. Therefore, the given equation holds. \square

Theorem A.1. *Let \mathbf{x} and \mathbf{y} be real-valued multivariate normal random vectors with $\mathbf{x} \sim N(\boldsymbol{\mu}_{\mathbf{x}}, \boldsymbol{\Sigma}_{\mathbf{x}})$, $\mathbf{y} \sim N(\boldsymbol{\mu}_{\mathbf{y}}, \boldsymbol{\Sigma}_{\mathbf{y}})$, and $\text{Cov}(\mathbf{x}, \mathbf{y}) = \boldsymbol{\Sigma}_{\mathbf{x}\mathbf{y}}$. For real (or complex) matrices $\mathbf{A}, \mathbf{B}, \mathbf{C}, \mathbf{D}$, and real (or complex) vectors $\mathbf{a}, \mathbf{b}, \mathbf{c}, \mathbf{d}$, the following equation holds.*

$$\begin{aligned} & E\left((\mathbf{A}\mathbf{x} + \mathbf{a})(\mathbf{B}\mathbf{y} + \mathbf{b})^\top (\mathbf{C}\mathbf{x} + \mathbf{c})(\mathbf{D}\mathbf{y} + \mathbf{d})^\top\right) \\ &= (\mathbf{A}\boldsymbol{\Sigma}_{\mathbf{x}\mathbf{y}}\mathbf{B}^\top + (\mathbf{A}\boldsymbol{\mu}_{\mathbf{x}} + \mathbf{a})(\mathbf{B}\boldsymbol{\mu}_{\mathbf{y}} + \mathbf{b})^\top)(\mathbf{C}\boldsymbol{\Sigma}_{\mathbf{x}\mathbf{y}}\mathbf{D}^\top + (\mathbf{C}\boldsymbol{\mu}_{\mathbf{x}} + \mathbf{c})(\mathbf{D}\boldsymbol{\mu}_{\mathbf{y}} + \mathbf{d})^\top) \\ &+ (\mathbf{A}\boldsymbol{\Sigma}_{\mathbf{x}}\mathbf{C}^\top + (\mathbf{A}\boldsymbol{\mu}_{\mathbf{x}} + \mathbf{a})(\mathbf{C}\boldsymbol{\mu}_{\mathbf{x}} + \mathbf{c})^\top)(\mathbf{B}\boldsymbol{\Sigma}_{\mathbf{y}}\mathbf{D}^\top + (\mathbf{B}\boldsymbol{\mu}_{\mathbf{y}} + \mathbf{b})(\mathbf{D}\boldsymbol{\mu}_{\mathbf{y}} + \mathbf{d})^\top) \\ &+ \text{tr}(\mathbf{B}^\top \mathbf{C}\boldsymbol{\Sigma}_{\mathbf{x}\mathbf{y}})(\mathbf{A}\boldsymbol{\Sigma}_{\mathbf{x}\mathbf{y}}\mathbf{D}^\top + (\mathbf{A}\boldsymbol{\mu}_{\mathbf{x}} + \mathbf{a})(\mathbf{D}\boldsymbol{\mu}_{\mathbf{y}} + \mathbf{d})^\top) \\ &+ (\mathbf{B}\boldsymbol{\mu}_{\mathbf{y}} + \mathbf{b})^\top (\mathbf{C}\boldsymbol{\mu}_{\mathbf{x}} + \mathbf{c})(\mathbf{A}\boldsymbol{\Sigma}_{\mathbf{x}\mathbf{y}}\mathbf{D}^\top - (\mathbf{A}\boldsymbol{\mu}_{\mathbf{x}} + \mathbf{a})(\mathbf{D}\boldsymbol{\mu}_{\mathbf{y}} + \mathbf{d})^\top). \end{aligned}$$

Proof. We follow a similar process of proof as described in Brookes (2020). Let $\mathbf{u} = \mathbf{x} - \boldsymbol{\mu}_{\mathbf{x}}$ and $\mathbf{v} = \mathbf{y} - \boldsymbol{\mu}_{\mathbf{y}}$. Then, $\mathbf{u} \sim N(\mathbf{0}, \boldsymbol{\Sigma}_{\mathbf{x}})$, $\mathbf{v} \sim N(\mathbf{0}, \boldsymbol{\Sigma}_{\mathbf{y}})$, and $\text{Cov}(\mathbf{u}, \mathbf{v}) = \boldsymbol{\Sigma}_{\mathbf{x}\mathbf{y}}$. Let us compute $E\left((\mathbf{A}\mathbf{u} + \mathbf{a})(\mathbf{B}\mathbf{v} + \mathbf{b})^\top (\mathbf{C}\mathbf{u} + \mathbf{c})(\mathbf{D}\mathbf{v} + \mathbf{d})^\top\right)$ first. When we multiply out the quartic expression and compute expectations of each term, we can remove odd-powered

terms involving \mathbf{u} and \mathbf{v} by applying Lemma A.1. Consequently, we get

$$\begin{aligned} & E\left((\mathbf{A}\mathbf{u} + \mathbf{a})(\mathbf{B}\mathbf{v} + \mathbf{b})^\top(\mathbf{C}\mathbf{u} + \mathbf{c})(\mathbf{D}\mathbf{v} + \mathbf{d})^\top\right) \\ &= E(\mathbf{A}\mathbf{u}\mathbf{v}^\top\mathbf{B}^\top\mathbf{C}\mathbf{u}\mathbf{v}^\top\mathbf{D}^\top) + E(\mathbf{A}\mathbf{u}\mathbf{v}^\top\mathbf{B}^\top\mathbf{c}\mathbf{d}^\top) + E(\mathbf{A}\mathbf{u}\mathbf{b}^\top\mathbf{C}\mathbf{u}\mathbf{d}^\top) + E(\mathbf{A}\mathbf{u}\mathbf{b}^\top\mathbf{c}\mathbf{v}^\top\mathbf{D}^\top) \\ &\quad + E(\mathbf{a}\mathbf{v}^\top\mathbf{B}^\top\mathbf{C}\mathbf{u}\mathbf{d}^\top) + E(\mathbf{a}\mathbf{v}^\top\mathbf{B}^\top\mathbf{c}\mathbf{v}^\top\mathbf{D}^\top) + E(\mathbf{a}\mathbf{b}^\top\mathbf{C}\mathbf{u}\mathbf{v}^\top\mathbf{D}^\top) + \mathbf{a}\mathbf{b}^\top\mathbf{c}\mathbf{d}^\top. \end{aligned}$$

By Lemma A.2, the first term in the right-hand side of the above equation is equal to $\mathbf{A}\Sigma_{\mathbf{x}\mathbf{y}}\mathbf{B}^\top\mathbf{C}\Sigma_{\mathbf{x}\mathbf{y}}\mathbf{D}^\top + \mathbf{A}\Sigma_{\mathbf{x}}\mathbf{C}^\top\mathbf{B}\Sigma_{\mathbf{y}}\mathbf{D}^\top + \mathbf{A}\Sigma_{\mathbf{x}\mathbf{y}}\mathbf{D}^\top \text{tr}(\mathbf{B}^\top\mathbf{C}\Sigma_{\mathbf{x}\mathbf{y}})$. By appropriately moving and transposing scalar factors and utilizing the property of the trace, the other terms on the right-hand side can be easily computed. As a result, we obtain

$$\begin{aligned} & E\left((\mathbf{A}\mathbf{u} + \mathbf{a})(\mathbf{B}\mathbf{v} + \mathbf{b})^\top(\mathbf{C}\mathbf{u} + \mathbf{c})(\mathbf{D}\mathbf{v} + \mathbf{d})^\top\right) \\ &= \mathbf{A}\Sigma_{\mathbf{x}\mathbf{y}}\mathbf{B}^\top\mathbf{C}\Sigma_{\mathbf{x}\mathbf{y}}\mathbf{D}^\top + \mathbf{A}\Sigma_{\mathbf{x}}\mathbf{C}^\top\mathbf{B}\Sigma_{\mathbf{y}}\mathbf{D}^\top + \mathbf{A}\Sigma_{\mathbf{x}\mathbf{y}}\mathbf{D}^\top \text{tr}(\mathbf{B}^\top\mathbf{C}\Sigma_{\mathbf{x}\mathbf{y}}) \\ &\quad + \mathbf{A}\Sigma_{\mathbf{x}\mathbf{y}}\mathbf{B}^\top\mathbf{c}\mathbf{d}^\top + \mathbf{A}\mathbf{C}_{\mathbf{x}}\mathbf{C}^\top\mathbf{b}\mathbf{d}^\top + \mathbf{b}^\top\mathbf{c}\mathbf{A}\Sigma_{\mathbf{x}\mathbf{y}}\mathbf{D}^\top \\ &\quad + \mathbf{a}\mathbf{d}^\top \text{tr}(\mathbf{B}^\top\mathbf{C}\Sigma_{\mathbf{x}\mathbf{y}}) + \mathbf{a}\mathbf{c}^\top\mathbf{B}\mathbf{C}_{\mathbf{y}}\mathbf{D}^\top + \mathbf{a}\mathbf{b}^\top\mathbf{C}\Sigma_{\mathbf{x}\mathbf{y}}\mathbf{D}^\top + \mathbf{a}\mathbf{b}^\top\mathbf{c}\mathbf{d}^\top \\ &= (\mathbf{A}\Sigma_{\mathbf{x}\mathbf{y}}\mathbf{B}^\top + \mathbf{a}\mathbf{b}^\top)(\mathbf{C}\Sigma_{\mathbf{x}\mathbf{y}}\mathbf{D}^\top + \mathbf{c}\mathbf{d}^\top) + (\mathbf{A}\Sigma_{\mathbf{x}}\mathbf{C}^\top + \mathbf{a}\mathbf{c}^\top)(\mathbf{B}\Sigma_{\mathbf{y}}\mathbf{D}^\top + \mathbf{b}\mathbf{d}^\top) \\ &\quad + \text{tr}(\mathbf{B}^\top\mathbf{C}\Sigma_{\mathbf{x}\mathbf{y}})(\mathbf{A}\Sigma_{\mathbf{x}\mathbf{y}}\mathbf{D}^\top + \mathbf{a}\mathbf{d}^\top) + \mathbf{b}^\top\mathbf{c}(\mathbf{A}\Sigma_{\mathbf{x}\mathbf{y}}\mathbf{D}^\top - \mathbf{a}\mathbf{d}^\top). \end{aligned}$$

Now, to prove the original statement, we replace $\mathbf{a}, \mathbf{b}, \mathbf{c}, \mathbf{d}$ by $\mathbf{A}\boldsymbol{\mu}_{\mathbf{x}} + \mathbf{a}, \mathbf{B}\boldsymbol{\mu}_{\mathbf{y}} + \mathbf{b}, \mathbf{C}\boldsymbol{\mu}_{\mathbf{x}} + \mathbf{c}, \mathbf{D}\boldsymbol{\mu}_{\mathbf{y}} + \mathbf{d}$, respectively. By utilizing the fact that $\mathbf{A}\mathbf{x} + \mathbf{a} = \mathbf{A}\mathbf{u} + (\mathbf{A}\boldsymbol{\mu}_{\mathbf{x}} + \mathbf{a})$, we complete the proof. \square

Corollary A.1. *Let \mathbf{x} and \mathbf{y} be real-valued multivariate normal random vectors with $\mathbf{x} \sim N(\mathbf{0}, \Sigma_{\mathbf{x}})$, $\mathbf{y} \sim N(\mathbf{0}, \Sigma_{\mathbf{y}})$, and $\text{Cov}(\mathbf{x}, \mathbf{y}) = \Sigma_{\mathbf{x}\mathbf{y}}$. For real (or complex) matrices \mathbf{A} , the following equation holds.*

$$E(\mathbf{x}\mathbf{y}^\top\mathbf{A}\mathbf{x}\mathbf{y}^\top) = \Sigma_{\mathbf{x}\mathbf{y}}\mathbf{A}\Sigma_{\mathbf{x}\mathbf{y}} + \Sigma_{\mathbf{x}}\mathbf{A}^\top\Sigma_{\mathbf{y}} + \text{tr}(\mathbf{A}\Sigma_{\mathbf{x}\mathbf{y}})\Sigma_{\mathbf{x}\mathbf{y}}.$$

Proof. It is clear from Theorem A.1. \square

We can now prove Proposition 3.6.

Proof. (a) It is easy to show by the following.

$$E(\hat{\mathbf{p}}_{XY}) = \text{diag}(\mathbf{V}^H E(\hat{\boldsymbol{\Sigma}}_{XY}) \mathbf{V}) = \text{diag}(\mathbf{V}^H \boldsymbol{\Sigma}_{XY} \mathbf{V}) = \mathbf{p}_{XY}.$$

(b) We start by computing

$$E\left((\hat{\mathbf{p}}_{XY})(\hat{\mathbf{p}}_{XY})^H\right) = \frac{1}{R^2} \sum_{r=1}^R \sum_{r'=1}^R E\left(\text{diag}(\mathbf{V}^H \mathbf{x}_r \mathbf{y}_r^H \mathbf{V}) \text{diag}(\mathbf{V}^H \mathbf{x}_{r'} \mathbf{y}_{r'}^H \mathbf{V})^H\right).$$

If $r \neq r'$, we obtain that

$$\begin{aligned} E\left(\text{diag}(\mathbf{V}^H \mathbf{x}_r \mathbf{y}_r^H \mathbf{V}) \text{diag}(\mathbf{V}^H \mathbf{x}_{r'} \mathbf{y}_{r'}^H \mathbf{V})^H\right) &= E\left(\text{diag}(\mathbf{V}^H \mathbf{x}_r \mathbf{y}_r^H \mathbf{V})\right) E\left(\text{diag}(\mathbf{V}^H \mathbf{x}_{r'} \mathbf{y}_{r'}^H \mathbf{V})^H\right) \\ &= \text{diag}(\mathbf{V}^H \boldsymbol{\Sigma}_{XY} \mathbf{V}) \text{diag}(\mathbf{V}^H \boldsymbol{\Sigma}_{XY} \mathbf{V})^H \\ &= \mathbf{p}_{XY} \mathbf{p}_{XY}^H. \end{aligned}$$

If $r = r'$, $E(\text{diag}(\mathbf{V}^H \mathbf{x}_r \mathbf{y}_r^H \mathbf{V}) \text{diag}(\mathbf{V}^H \mathbf{x}_r \mathbf{y}_r^H \mathbf{V})^H)$ has its (i, j) th element equal to

$$E((\mathbf{v}_i^H \mathbf{x}_r \mathbf{y}_r^H \mathbf{v}_i)(\mathbf{v}_j^H \mathbf{x}_r \mathbf{y}_r^H \mathbf{v}_j)^*) = \mathbf{v}_i^H E(\mathbf{x}_r \mathbf{y}_r^H \mathbf{v}_i \mathbf{v}_j^\top \mathbf{x}_r^* \mathbf{y}_r^\top) \mathbf{v}_j^*,$$

where \mathbf{v}_i is the i th column of \mathbf{V} . Since \mathbf{x}_r and \mathbf{y}_r are real-valued, by Corollary A.1,

$$E(\mathbf{x}_r \mathbf{y}_r^H \mathbf{v}_i \mathbf{v}_j^\top \mathbf{x}_r^* \mathbf{y}_r^\top) = E(\mathbf{x}_r \mathbf{y}_r^\top \mathbf{v}_i \mathbf{v}_j^\top \mathbf{x}_r \mathbf{y}_r^\top) = \boldsymbol{\Sigma}_{XY} \mathbf{v}_i \mathbf{v}_j^\top \boldsymbol{\Sigma}_{XY} + \boldsymbol{\Sigma}_X \mathbf{v}_j \mathbf{v}_i^\top \boldsymbol{\Sigma}_Y + \text{tr}(\mathbf{v}_i \mathbf{v}_j^\top \boldsymbol{\Sigma}_{XY}) \boldsymbol{\Sigma}_{XY}.$$

Since \mathbf{S} is symmetric, \mathbf{V} is real matrix; thus,

$$E\left((\mathbf{v}_i^H \mathbf{x}_r \mathbf{y}_r^H \mathbf{v}_i)(\mathbf{v}_j^H \mathbf{x}_r \mathbf{y}_r^H \mathbf{v}_j)^*\right) = \begin{cases} 2|(\mathbf{p}_{XY})_i|^2 + (\mathbf{p}_X)_i (\mathbf{p}_Y)_i & \text{if } i = j, \\ (\mathbf{p}_{XY})_i (\mathbf{p}_{XY}^*)_j & \text{if } i \neq j. \end{cases}$$

Combining these results together, we can compute $E((\hat{\mathbf{p}}_{XY})(\hat{\mathbf{p}}_{XY})^H)$, and obtain

$$\text{Var}(\hat{\mathbf{p}}_{XY}) = E\left((\hat{\mathbf{p}}_{XY})(\hat{\mathbf{p}}_{XY})^H\right) - \mathbf{p}_{XY} \mathbf{p}_{XY}^H = \frac{1}{R} \left(\text{diag}(|\mathbf{p}_{XY}|^2) + \text{diag}(\mathbf{p}_X) \text{diag}(\mathbf{p}_Y)\right).$$

□

A.7 Proof of Proposition 3.7

Proof. We can rewrite $\hat{\mathbf{p}}_{XY}^w = \text{diag}(\tilde{\mathbf{W}}\mathbf{V}^H\mathbf{x}\mathbf{y}^H\mathbf{V}\tilde{\mathbf{W}}^H)$. Then, the following equation can be obtained by taking expectation

$$E(\hat{\mathbf{p}}_{XY}^w) = \text{diag}(\tilde{\mathbf{W}}\mathbf{V}^H\Sigma_{XY}\mathbf{V}\tilde{\mathbf{W}}^H) = \text{diag}(\tilde{\mathbf{W}}\text{diag}(\mathbf{p}_{XY})\tilde{\mathbf{W}}^H) = (\tilde{\mathbf{W}} \circ \tilde{\mathbf{W}}^*)\mathbf{p}_{XY}.$$

The proof is completed. \square

A.8 Proof of Proposition 3.8

Proof. (a) The proof for the expectation follows the same approach to the proof of Proposition 3.7.

(b) To compute the trace of the covariance matrix, we focus on the diagonal elements of $\text{Var}(\hat{\mathbf{p}}_{XY}^w)$. For $1 \leq i \leq N$, compute $E\left(\left(\hat{\mathbf{p}}_{XY}^w\right)_{i,i}\right) = E\left(\left(\hat{\mathbf{p}}_{XY}^w\right)_i\left(\hat{\mathbf{p}}_{XY}^w\right)_i^*\right)$ as

$$\begin{aligned} E\left(\left(\hat{\mathbf{p}}_{XY}^w\right)_i\left(\hat{\mathbf{p}}_{XY}^w\right)_i^*\right) &= E\left(\frac{1}{M}\sum_{m=1}^M(\tilde{\mathbf{W}}_{m,i}^\top\tilde{\mathbf{x}})(\tilde{\mathbf{W}}_{m,i}^\top\tilde{\mathbf{y}})^*\frac{1}{M}\sum_{m'=1}^M(\tilde{\mathbf{W}}_{m',i}^\top\tilde{\mathbf{x}})^*(\tilde{\mathbf{W}}_{m',i}^\top\tilde{\mathbf{y}})\right) \\ &= \frac{1}{M^2}\sum_{m=1}^M\sum_{m'=1}^M\tilde{\mathbf{W}}_{m,i}^\top E(\tilde{\mathbf{x}}\tilde{\mathbf{y}}^H\tilde{\mathbf{W}}_{m,i}^*\tilde{\mathbf{W}}_{m',i}^H\tilde{\mathbf{x}}^*\tilde{\mathbf{y}}^\top)\tilde{\mathbf{W}}_{m',i}, \end{aligned}$$

where $\tilde{\mathbf{W}}_{m,i}^\top$ is the i th row vector of $\tilde{\mathbf{W}}_m$, $\tilde{\mathbf{x}} = \mathbf{V}^H\mathbf{x}$, and $\tilde{\mathbf{y}} = \mathbf{V}^H\mathbf{y}$. Since \mathbf{S} is symmetric, \mathbf{V} is real matrix. Therefore, $\tilde{\mathbf{x}}$ and $\tilde{\mathbf{y}}$ are zero-mean real-valued multivariate normal random vectors, allowing us to utilize Corollary A.1 to evaluate $E(\tilde{\mathbf{x}}\tilde{\mathbf{y}}^H\tilde{\mathbf{W}}_{m,i}^*\tilde{\mathbf{W}}_{m',i}^H\tilde{\mathbf{x}}^*\tilde{\mathbf{y}}^\top)$, in conjunction with the results from Property 3 in Segarra et al. (2016) and Proposition 3.4.

$$\begin{aligned} E(\tilde{\mathbf{x}}\tilde{\mathbf{y}}^H\tilde{\mathbf{W}}_{m,i}^*\tilde{\mathbf{W}}_{m',i}^H\tilde{\mathbf{x}}^*\tilde{\mathbf{y}}^\top) &= \text{diag}(\mathbf{p}_{XY})\tilde{\mathbf{W}}_{m,i}^*\tilde{\mathbf{W}}_{m',i}^H\text{diag}(\mathbf{p}_{XY}) + \text{diag}(\mathbf{p}_X)\tilde{\mathbf{W}}_{m',i}^*\tilde{\mathbf{W}}_{m,i}^H\text{diag}(\mathbf{p}_Y) \\ &\quad + \text{tr}(\tilde{\mathbf{W}}_{m,i}^*\tilde{\mathbf{W}}_{m',i}^H\text{diag}(\mathbf{p}_{XY}))\text{diag}(\mathbf{p}_{XY}). \end{aligned}$$

Then, by appropriately transposing scalar factors and utilizing the property of the trace, we obtain

$$\begin{aligned}\tilde{\mathbf{W}}_{m,i}^\top E(\tilde{\mathbf{x}}\tilde{\mathbf{y}}^H \tilde{\mathbf{W}}_{m,i}^* \tilde{\mathbf{W}}_{m',i}^H \tilde{\mathbf{x}}^* \tilde{\mathbf{y}}^\top) \tilde{\mathbf{W}}_{m',i} &= \tilde{\mathbf{W}}_{m,i}^\top \text{diag}(\mathbf{p}_{XY}) \tilde{\mathbf{W}}_{m,i}^* \tilde{\mathbf{W}}_{m',i}^H \text{diag}(\mathbf{p}_{XY}) \tilde{\mathbf{W}}_{m',i} \\ &+ \tilde{\mathbf{W}}_{m,i}^\top \text{diag}(\mathbf{p}_X) \tilde{\mathbf{W}}_{m',i}^* \tilde{\mathbf{W}}_{m,i}^H \text{diag}(\mathbf{p}_Y) \tilde{\mathbf{W}}_{m',i} \\ &+ |\tilde{\mathbf{W}}_{m,i}^\top \text{diag}(\mathbf{p}_{XY}) \tilde{\mathbf{W}}_{m',i}^*|^2.\end{aligned}$$

Now, let us evaluate $|E((\hat{\mathbf{p}}_{XY}^{\mathcal{W}})_i)|^2$.

$$\begin{aligned}|E((\hat{\mathbf{p}}_{XY}^{\mathcal{W}})_i)|^2 &= E\left(\frac{1}{M} \sum_{m=1}^M (\tilde{\mathbf{W}}_{m,i}^\top \tilde{\mathbf{x}}) (\tilde{\mathbf{W}}_{m,i}^\top \tilde{\mathbf{y}})^*\right) E\left(\frac{1}{M} \sum_{m'=1}^M (\tilde{\mathbf{W}}_{m',i}^\top \tilde{\mathbf{x}})^* (\tilde{\mathbf{W}}_{m',i}^\top \tilde{\mathbf{y}})\right) \\ &= \frac{1}{M^2} \sum_{m=1}^M \sum_{m'=1}^M \tilde{\mathbf{W}}_{m,i}^\top \text{diag}(\mathbf{p}_{XY}) \tilde{\mathbf{W}}_{m,i}^* \tilde{\mathbf{W}}_{m',i}^H \text{diag}(\mathbf{p}_{XY}) \tilde{\mathbf{W}}_{m',i}.\end{aligned}$$

Thus,

$$\begin{aligned}(\text{Var}(\hat{\mathbf{p}}_{XY}^{\mathcal{W}}))_{i,i} &= E\left((\hat{\mathbf{p}}_{XY}^{\mathcal{W}})_i (\hat{\mathbf{p}}_{XY}^{\mathcal{W}})_i^*\right) - |E((\hat{\mathbf{p}}_{XY}^{\mathcal{W}})_i)|^2 \\ &= \frac{1}{M^2} \sum_{m=1}^M \sum_{m'=1}^M \left(\tilde{\mathbf{W}}_{m,i}^\top \text{diag}(\mathbf{p}_X) \tilde{\mathbf{W}}_{m',i}^* \tilde{\mathbf{W}}_{m,i}^H \text{diag}(\mathbf{p}_Y) \tilde{\mathbf{W}}_{m',i} + |\tilde{\mathbf{W}}_{m,i}^\top \text{diag}(\mathbf{p}_{XY}) \tilde{\mathbf{W}}_{m',i}^*|^2\right) \\ &= \frac{1}{M^2} \sum_{m=1}^M \sum_{m'=1}^M \left(\langle (\tilde{\mathbf{W}}_{m,m'} \mathbf{p}_X)_i, (\tilde{\mathbf{W}}_{m,m'} \mathbf{p}_Y)_i \rangle + |(\tilde{\mathbf{W}}_{m,m'} \mathbf{p}_{XY})_i|^2\right).\end{aligned}$$

Therefore, the proof is completed as follows.

$$\text{tr}(\text{Var}(\hat{\mathbf{p}}_{XY}^{\mathcal{W}})) = \frac{1}{M^2} \sum_{m=1}^M \sum_{m'=1}^M \text{tr}\left((\tilde{\mathbf{W}}_{m,m'} \mathbf{p}_{XY})(\tilde{\mathbf{W}}_{m,m'} \mathbf{p}_{XY})^H + (\tilde{\mathbf{W}}_{m,m'} \mathbf{p}_X)(\tilde{\mathbf{W}}_{m,m'} \mathbf{p}_Y)^H\right).$$

□

A.9 Proof of Proposition 3.9

Proof. It is directly extended from the proof of Proposition 5 in Marques et al. (2017) by Proposition 3.3. □

A.10 Proof of Proposition 3.10

Proof. For a given $1 \leq i \leq N$, we know that $|(\mathbf{p}_{XY})_i|^2 = |(E(\tilde{X}\tilde{Y}^H))_{i,i}|^2 = |E(\tilde{X}_i\tilde{Y}_i^*)|^2$ from Proposition 3.4, where \tilde{X}_i and \tilde{Y}_i represent the i th elements of the GFT processes \tilde{X} and \tilde{Y} , respectively. Similarly, $(\mathbf{p}_X)_i = E(\tilde{X}_i\tilde{X}_i^*)$ and $(\mathbf{p}_Y)_i = E(\tilde{Y}_i\tilde{Y}_i^*)$. Therefore, it is clear that $0 \leq \mathbf{c}_{XY}$. Moreover, by the Cauchy-Schwarz inequality, it also holds that $\mathbf{c}_{XY} \leq \mathbf{1}$.

To satisfy the equality $\mathbf{c}_{XY} = \mathbf{0}$, $E(\tilde{X}_i\tilde{Y}_i^*)$ should be zero for all i . It is equivalent to $\mathbf{p}_{XY} = \mathbf{0}$ from Proposition 3.4, which is also equivalent to $\mathbf{\Sigma}_{XY}$ being a zero matrix. Thus, the equality $\mathbf{c}_{XY} = \mathbf{0}$ holds when X and Y are uncorrelated. To satisfy the equality $\mathbf{c}_{XY} = \mathbf{1}$, $\tilde{Y}_i = \alpha_i\tilde{X}_i$ for some constant α_i for all i . It is satisfied when $Y = \mathbf{H}X$ for a filter \mathbf{H} with frequency response $\tilde{\mathbf{h}}_i = \alpha_i$, and the proof is complete. \square

References

- Anis, A. and Ortega, A. (2017). Critical sampling for wavelet filterbanks on arbitrary graphs. In *2017 IEEE International Conference on Acoustics, Speech and Signal Processing (ICASSP)*, pages 3889–3893. IEEE.
- Bartlett, M. S. (1950). Periodogram analysis and continuous spectra. *Biometrika*, 37(1/2):1–16.
- Blackman, R. and Tukey, J. (1959). *The Measurement of Power Spectra From the Point of View of Communications Engineering*. Dover Publications.
- Brookes, M. (2020). The matrix reference manual. [online] <http://www.ee.imperial.ac.uk/hp/staff/dmb/matrix/intro.html>.
- Bulai, I. M. and Saliiani, S. (2023). Spectral graph wavelet packets frames. *Applied and Computational Harmonic Analysis*, 66:18–45.
- Canbolat, A. and Vural, E. (2024). Locally stationary graph processes. *IEEE Transactions on Signal Processing*, 72:2323–2332.
- Chen, S., Sandryhaila, A., Moura, J. M., and Kovačević, J. (2015a). Signal recovery on graphs: Variation minimization. *IEEE Transactions on Signal Processing*, 63(17):4609–4624.
- Chen, S., Varma, R., Sandryhaila, A., and Kovačević, J. (2015b). Discrete signal processing on graphs: Sampling theory. *IEEE Transactions on Signal Processing*, 63(24):6510–6523.
- Crovella, M. and Kolaczyk, E. (2003). Graph wavelets for spatial traffic analysis. In *IEEE INFOCOM 2003. Twenty-second Annual Joint Conference of the IEEE Computer and Communications Societies*, volume 3, pages 1848–1857. IEEE.
- Fuller, W. A. (2009). *Introduction to Statistical Time Series*. John Wiley & Sons.
- Girault, B. (2015a). *Signal Processing on Graphs-Contributions to An Emerging Field*. PhD thesis, Ecole normale supérieure de lyon-ENS LYON.

- Girault, B. (2015b). Stationary graph signals using an isometric graph translation. In *2015 23rd European Signal Processing Conference (EUSIPCO)*, pages 1516–1520. IEEE.
- Hammond, D. K., Vandergheynst, P., and Gribonval, R. (2011). Wavelets on graphs via spectral graph theory. *Applied and Computational Harmonic Analysis*, 30(2):129–150.
- Huber, P. J. (1964). Robust estimation of a location parameter. *Annals of Mathematical Statistics*, 35(1):73–101.
- Isserlis, L. (1918). On a formula for the product-moment coefficient of any order of a normal frequency distribution in any number of variables. *Biometrika*, 12(1/2):134–139.
- Kim, K. and Oh, H.-S. (2024). Network time series forecasting using spectral graph wavelet transform. *International Journal of Forecasting*.
- Lorenzo, P., Barbarossa, S., and Banelli, P. (2018). Sampling and recovery of graph signals. In *Cooperative and Graph Signal Processing*, pages 261–282. Elsevier.
- Loukas, A. and Perraudin, N. (2019). Stationary time-vertex signal processing. *EURASIP Journal on Advances in Signal Processing*, 2019(1):1–19.
- Marques, A. G., Segarra, S., Leus, G., and Ribeiro, A. (2017). Stationary graph processes and spectral estimation. *IEEE Transactions on Signal Processing*, 65(22):5911–5926.
- Narang, S. K. and Ortega, A. (2009). Lifting based wavelet transforms on graphs. In *Proceedings: Asia-Pacific Signal and Information Processing Association, 2009 Annual Summit and Conference*, pages 441–444. Asia-Pacific Signal and Information Processing Association.
- Narang, S. K. and Ortega, A. (2011). Downsampling graphs using spectral theory. In *2011 IEEE International Conference on Acoustics, Speech and Signal Processing (ICASSP)*, pages 4208–4211. IEEE.
- Narang, S. K. and Ortega, A. (2012). Perfect reconstruction two-channel wavelet filter

- banks for graph structured data. *IEEE Transactions on Signal Processing*, 60(6):2786–2799.
- Onuki, M., Ono, S., Yamagishi, M., and Tanaka, Y. (2016). Graph signal denoising via trilateral filter on graph spectral domain. *IEEE Transactions on Signal and Information Processing over Networks*, 2(2):137–148.
- Perraudin, N. and Vandergheynst, P. (2017). Stationary signal processing on graphs. *IEEE Transactions on Signal Processing*, 65(13):3462–3477.
- Phillips, G. M. (2006). *Interpolation and Approximation by Polynomials*. Springer Science & Business Media.
- Priestley, M. (1982). *Spectral Analysis and Time Series, Two-Volume Set: Volumes I and II*. Elsevier Science.
- Sakiyama, A. and Tanaka, Y. (2014). Oversampled graph laplacian matrix for graph filter banks. *IEEE Transactions on Signal Processing*, 62(24):6425–6437.
- Sandryhaila, A. and Moura, J. M. (2013a). Discrete signal processing on graphs. *IEEE Transactions on Signal Processing*, 61(7):1644–1656.
- Sandryhaila, A. and Moura, J. M. (2013b). Discrete signal processing on graphs: Graph Fourier transform. In *2013 IEEE International Conference on Acoustics, Speech, and Signal Processing*, pages 6167–6170. IEEE.
- Sandryhaila, A. and Moura, J. M. (2014). Discrete signal processing on graphs: Frequency analysis. *IEEE Transactions on Signal Processing*, 62(12):3042–3054.
- Segarra, S., Chepuri, S. P., Marques, A. G., and Leus, G. (2018). Statistical graph signal processing: Stationarity and spectral estimation. In *Cooperative and Graph Signal Processing*, pages 325–347. Elsevier.
- Segarra, S., Marques, A. G., Leus, G., and Ribeiro, A. (2016). Stationary graph processes: Nonparametric spectral estimation. In *2016 IEEE Sensor Array and Multichannel Signal Processing Workshop (SAM)*, pages 1–5. IEEE.

- Shuman, D. I., Ricaud, B., and Vandergheynst, P. (2016). Vertex-frequency analysis on graphs. *Applied and Computational Harmonic Analysis*, 40(2):260–291.
- Stankovic, L., Mandic, D., Dakovic, M., Brajovic, M., Scalzo, B., and Constantinides, A. G. (2019). Graph signal processing—part ii: Processing and analyzing signals on graphs. *arXiv preprint arXiv:1909.10325*.
- Tanaka, Y. (2018). Spectral domain sampling of graph signals. *IEEE Transactions on Signal Processing*, 66(14):3752–3767.
- Tremblay, N., Gonçalves, P., and Borgnat, P. (2018). Design of graph filters and filterbanks. In *Cooperative and Graph Signal Processing*, pages 299–324. Elsevier.
- Von Storch, H. and Zwiers, F. W. (2002). *Statistical Analysis in Climate Research*. Cambridge University Press.
- Waheed, W. and Tay, D. B. (2018). Graph polynomial filter for signal denoising. *IET Signal Processing*, 12(3):301–309.
- Welch, P. (1967). The use of fast fourier transform for the estimation of power spectra: A method based on time averaging over short, modified periodograms. *IEEE Transactions on Audio and Electroacoustics*, 15(2):70–73.
- Zachary, W. W. (1977). An information flow model for conflict and fission in small groups. *Journal of Anthropological Research*, 33(4):452–473.